

RL-TR-95-193
Final Technical Report
October 1995



MULTISTAGE OPTICAL INTERCONNECTS FOR PARALLEL ACCESS OPTICAL SHARED MEMORIES

University of California/San Diego

Yeshayahu Fainman

APPROVED FOR PUBLIC RELEASE; DISTRIBUTION UNLIMITED.

19960501 149

Rome Laboratory
Air Force Materiel Command
Griffiss Air Force Base, New York

DTIC QUALITY INSPECTED 1

This report has been reviewed by the Rome Laboratory Public Affairs Office (PA) and is releasable to the National Technical Information Service (NTIS). At NTIS it will be releasable to the general public, including foreign nations.

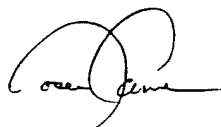
RL-TR-95-193 has been reviewed and is approved for publication.

APPROVED:



BERNARD J. CLARKE, Captain, USAF
Project Engineer

FOR THE COMMANDER:



JOSEPH CAMERA
Technical Director
Intelligence & Reconnaissance Directorate

If your address has changed or if you wish to be removed from the Rome Laboratory mailing list, or if the addressee is no longer employed by your organization, please notify RL (IRAP) Griffiss AFB NY 13441. This will assist us in maintaining a current mailing list.

Do not return copies of this report unless contractual obligations or notices on a specific document require that it be returned.

REPORT DOCUMENTATION PAGE			Form Approved OMB No. 0704-0188	
<small>Public reporting burden for this collection of information is estimated to average 1 hour per response, including the time for reviewing instructions, searching existing data sources, gathering and maintaining the data needed, and completing and reviewing the collection of information. Send comments regarding this burden estimate or any other aspect of the collection of information, including suggestions for reducing this burden, to Washington Headquarters Services, Directorate for Information Operations and Reports, 1215 Jefferson Davis Highway, Suite 1204, Arlington, VA 22202-4302, and to the Office of Management and Budget, Paperwork Reduction Project (0704-0188), Washington, DC 20503.</small>				
1. AGENCY USE ONLY (Leave Blank)		2. REPORT DATE October 1995		3. REPORT TYPE AND DATES COVERED Final Sep 91 - Mar 93
4. TITLE AND SUBTITLE MULTISTAGE OPTICAL INTERCONNECTS FOR PARALLEL ACCESS OPTICAL SHARED MEMORIES			5. FUNDING NUMBERS C - F30602-91-C-0094 PE - 62702F PR - 4594 TA - 15 WU - H4	
6. AUTHOR(S) Yeshayahu Fainman				
7. PERFORMING ORGANIZATION NAME(S) AND ADDRESS(ES) University of California/San Diego Lo Jolla CA 92093-0407			8. PERFORMING ORGANIZATION REPORT NUMBER N/A	
9. SPONSORING/MONITORING AGENCY NAME(S) AND ADDRESS(ES) Rome Laboratory (IRAP) 32 Hangar Rd Rome NY 13441-4514			10. SPONSORING/MONITORING AGENCY REPORT NUMBER RL-TR-95-193	
11. SUPPLEMENTARY NOTES Rome Laboratory Project Engineer: Bernard J. Clarke, Captain, USAF/IRAP/ (315) 330-4581				
12a. DISTRIBUTION/AVAILABILITY STATEMENT Approved for public release; distribution unlimited.			12b. DISTRIBUTION CODE	
13. ABSTRACT (Maximum 200 words) We have completed a network design study that identified the Dilated Benes network routing algorithm as the most compatible with this technology and that quantified the importance of BCGH performance in attaining large (≥ 1024 node) networks. We therefore placed more emphasis on achieving high efficiency and contrast ratio BCGH. The diffraction efficiency of the original binary phase LiNbO_3 element was increased from 6% to 60% by going to four phase level design, and transmission through uncoated elements was increased from 51% to >99% by antireflection coating. A contrast ratio between orthogonal polarizations of 160:1 was demonstrated with 60% diffraction efficiency. As a subsystem demonstration, we used two BCGH and a liquid crystal polarization rotator to create a 2x2 optical node that combined both routing and switching. We demonstrated switching contrast ratio of better than 50:1, and also used a high speed diode to show 20 MHz data modulation. We conclude that polarization-selective holographic optical elements with transmission and diffraction efficiencies approaching 100% require only fabrication refinements, and that such elements can become a key component of future optical systems, including a high bandwidth multistage interconnection network using polarization switching.				
14. SUBJECT TERMS Optical interconnects, Parallel access, Optical memories			15. NUMBER OF PAGES 80	
			16. PRICE CODE	
17. SECURITY CLASSIFICATION OF REPORT UNCLASSIFIED	18. SECURITY CLASSIFICATION OF THIS PAGE UNCLASSIFIED	19. SECURITY CLASSIFICATION OF ABSTRACT UNCLASSIFIED	20. LIMITATION OF ABSTRACT III	

ABSTRACT

We describe our research results and compare them to the goals stated in the original contract, concluding that the contract goals were successfully met. During the one year research program we have demonstrated a unique optical element capable of acting with an arbitrary independent phase function upon illumination with horizontally or vertically polarized monochromatic light. This element, called a BCGH (for birefringent computer generated hologram) is composed of two birefringent substrates, etched with a surface relief patterns and joined face to face. This is a new type of optical element which may be useful in a variety of coherent optical applications, especially when combined with a electro-optic polarization rotator such as a liquid crystal modulator. Our research application was a high speed parallel optical interconnection network for memory access.

We have completed a network design study which identified the Dilated Benes network routing algorithm as the most compatible with this technology, and which quantified the importance of BCGH performance in attaining large (≥ 1024 node) networks. We therefore placed more emphasis on achieving high efficiency and contrast ratio BCGH. The diffraction efficiency of the original binary phase LiNbO_3 element was increased from 6% to 60% by going to four phase level design, and transmission through uncoated elements was increased from 51% to >99% by antireflection coating. A contrast ratio between orthogonal polarizations of 160:1 was demonstrated with 60% diffraction efficiency. As a subsystem demonstration we used two BCGH and a liquid crystal polarization rotator to create a 2x2 optical node which combined both routing and switching. We demonstrated switching contrast ratio of better than 50:1, and also used a high speed diode laser source to show 20 MHz data modulation.

We conclude that polarization-selective holographic optical elements with transmission and diffraction efficiencies approaching 100% require only fabrication refinements, and that such elements can become a key component of future optical systems, including a high bandwidth multistage interconnection network using polarization switching.

Table of Contents

1. Overview	1
2. Architecture Design Study.....	2
2.1 BCGH Switching Element.....	3
2.2 Network Control Algorithms	4
2.3 Interconnection Network Topology	7
3. BCGH Element Fabrication	10
3.1 BCGH Design.....	10
3.2 BCGH Fabrication.....	13
3.3 BCGH Performance Improvements	16
4. Sub-System Demonstrations	19
4.1 1 × 2 Switch Demonstration	19
4.2 2 × 2 Switch Demonstration	20
4.3 Fast Data Transmission Demonstration	22
5. Conclusions.....	23
5.1 Summary of Accomplishments.....	23
5.2 Future Technology Development for Dual Use Applications.....	24
5.3 Acknowledgments.....	24
6. References	25
Appendices.....	26
A.1 Polarization-selective computer-generated holograms.....	26
A.2 Polarization-selective computer-generated holograms for optical multistage interconnection networks.....	30
A.3 Polarization selective computer generated holograms and applications	36
A.4 Architectural considerations for MINs based on BCGH technology ...	49

1. Overview

This final report will summarize the original program goals and the research results. For convenience, the publications^{1,2,3,4} and a technical report are included as appendices to this report.

The long-term project goal is to demonstrate a reconfigurable free space optical interconnection network suitable for parallel optical memory access. Our approach is a multistage interconnection network (MIN) using binary polarization switches and novel polarization-selective computer generated holograms (CGH) to switch and route the light at each node. The interconnection network will be circuit switched, and can be either locally or globally routed. The set-up time (latency) depends on the modulator technology, but the data modulation rate is limited only by the source modulation frequency, which can easily exceed 1 GHz and may approach THz rates as telecommunications technology advances. The key technology for this approach is a high efficiency holographic optical element which acts independently horizontally and vertically polarized inputs. Such an element would allow the network to be simple and compact, because each hologram replaces an entire subsystem of components required to build the network using conventional optics.

The most significant accomplishment of this program was the demonstration of a polarization selective component, called BCGH for birefringent computer generated hologram. The advantage of this element is shown in Figure 1, where the optical components necessary to separate horizontally and vertically polarized input into distinct paths, image each onto its own conventional computer generated hologram (CGH), and finally recombine them into the same image plane are compared to the single functionally identical BCGH element. The technology used is an extension of kinoform phase-only CGH, where an isotropic glass substrate is etched with a surface relief profile to obtain the desired phase profile. Instead of applying a single phase profile, however, we need to apply an independent profile for each polarization. The polarization dependence of BCGH comes from fabricating them in birefringent media. Two birefringent crystals etched with a surface-relief profile are cemented face-to-face to yield a single optical element which can have high diffraction efficiency and arbitrary functionality for each independent linear polarization.

The first year of the project had three goals: 1) perform an architecture design study to identify the network routing algorithm most compatible with this technology and quantify the effect of BCGH performance for large (≥ 1024 node) networks, 2) demonstrate working BCGH elements with the highest possible performance, and 3) use BCGH elements in small-scale interconnection. Final section concludes this report with an assessment of the potential of this new optical technology for this and other applications.

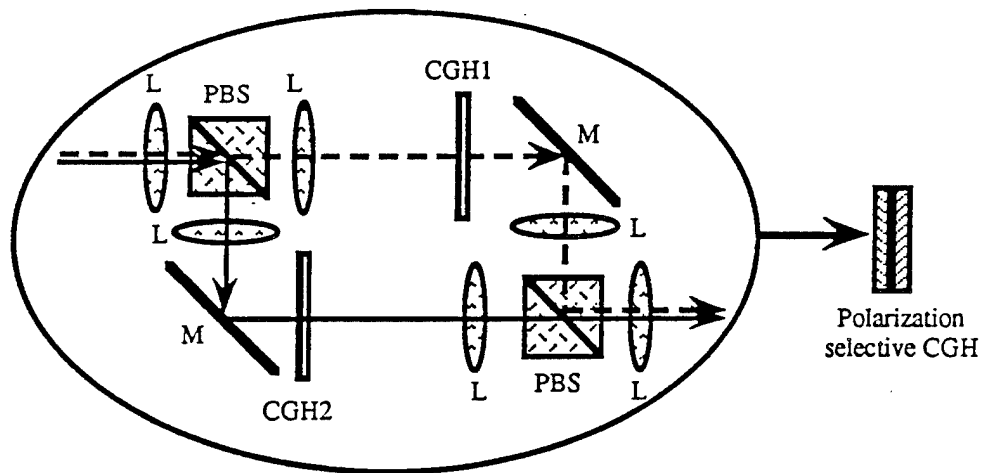


Figure 1: A single BCGH replaces up to 12 optical components with one compact element.

2. Architecture Design Study

The objective of the project was to design a high data rate multistage interconnection networks (MIN) that would far exceed the capabilities of state-of-the-art electronic networks. Existing designs for VLSI based interconnection networks can be separated into two main categories, MINs and crossbars. Both have been implemented only with VLSI to date. Crossbars were the first type of VLSI interconnection networks. They use nearest neighbor (mesh) interconnections in a $N \times N$ array of switches. 64×64 prototype chips with bandwidths in excess of 200 Mbits/channel have been demonstrated. The number of switches a signal passes through ranges from 1 to $2N-1$, introducing signal skew. Skew can only be corrected by slowing the network speed to the longest delay. Larger networks can be assembled from smaller crossbar chips with, however, a reduced bandwidth/channel. Electronic MINs were introduced to reduce the chip area dedicated to switches. They typically require $O(N \log_2 N)$ switches instead of N^2 for the crossbar. These networks have data rates in the 100 Mbit/sec range. Prototype VLSI chips with 32 inputs and 32 outputs (32×32) self-routing networks have been built. These networks can take up to several hundred inputs by use of several chips, again with an associated loss of bandwidth per channel. Such networks do not scale well, as the bandwidth/channel drops rapidly beyond network sizes of 256.

The locally-interconnected topology of a crossbar places more of the burden on processing area, while the globally-interconnected MIN puts the emphasis on interconnection wires. As the network size and longest line-length increase, the costs of communication in all-electronic processing tend to dominate. This makes crossbar networks the most effective approach for large-scale applications. However, if the communication costs could be reduced then the primary advantage of MINs, the lower switch count, would make them more attractive than crossbars. Optical interconnection offers the

potential for a significant reduction in communication costs, especially at the long distances characteristic of large interconnection networks.

Based on these considerations, to be competitive with VLSI we need either: (1) Network size $N > 256$ I/O channels with bandwidth/channel > 100 Mbits/sec, (2) Network size $N > 64$ I/O channels with bandwidth/channel > 500 Mbits/sec, or (3) Any size network with data rates in excess of 1 Gbit/sec. We must also consider other competitive technologies, such as GaAs, which might provide Gbit/sec links. Therefore we chose alternative (3). Our goal is an interconnection network with $N \geq 256$ channels and $BW / \text{channel} \geq 1 \text{ Gbit/sec}$.

2.1 BCGH Switching Element

A single BCGH switching element is shown in Figure 2. The function of the optical switch is to (i) take two optical data inputs, with orthogonal polarizations, entering from two directions, then (ii) either exchange them or not, depending on the switch setting, and finally (iii) direct them towards the appropriate destinations in the next stage of the MIN. The switch consists of a BCGH which combines the inputs, an active polarization rotator to exchange the inputs, and a second BCGH to direct the output. The sources of optical loss are reflections from the dielectric surfaces and the diffraction efficiency of the holograms. A silicon processing chip is necessary for smart SLM operation. Depending on the particular device technology, this will introduce additional surfaces (for example, a common sapphire substrate holding both the silicon and modulator materials) or not (if a silicon chip with openings etched into it acts as the substrate). However, the calculations presented here are representative of the realistic switch performance obtainable.

Surface reflections losses come from the BCGH substrate (R_g) and the modulator substrate (R_m). Clipping loss C occurs when the beams are focused through an aperture at the modulator. The finally source of loss is the diffraction efficiency of the holograms η . Total switch efficiency is then $\eta_{\text{switch}} = \eta^2 R_g^8 R_m^2 C$. Assuming that each optical surface is antireflection coated with a single dielectric layer (for maximum input angle range), and a 16-level phase hologram is used, then these constants can be estimated to be $\eta = 98.7\%$, $R_g = R_m = 99\%$, and $C = 98.6\%$. The total switch efficiency would then be 86.9% , for an insertion loss of $10\log_{10}[\eta_{\text{switch}}] = -0.612 \text{ dB}$.

If the polarization rotation was perfect and the BCGHs distinguished completely between the two polarizations the crosstalk would be zero and the network's SNR would be infinite. Of course, they are not. We define the crosstalk coming from one switch as δ_c , then define S to be the maximum number of switches in one path and P_o to be the maximum signal strength (when crosstalk is worst). Then the SNR of the entire network is given by $\text{SNR}_{\text{network}} = \log_{10}(1/\delta_c) - \log_{10}S$. δ_c is a critical factor that will determine the choice of architecture and maximum network size. In our calculations, we considered two

examples: $\delta_c = 0.1\%$ and $\delta_c = 1\%$. These two cases may be typical of currently achievable technology for bulk and pixellated BCGH switching elements.

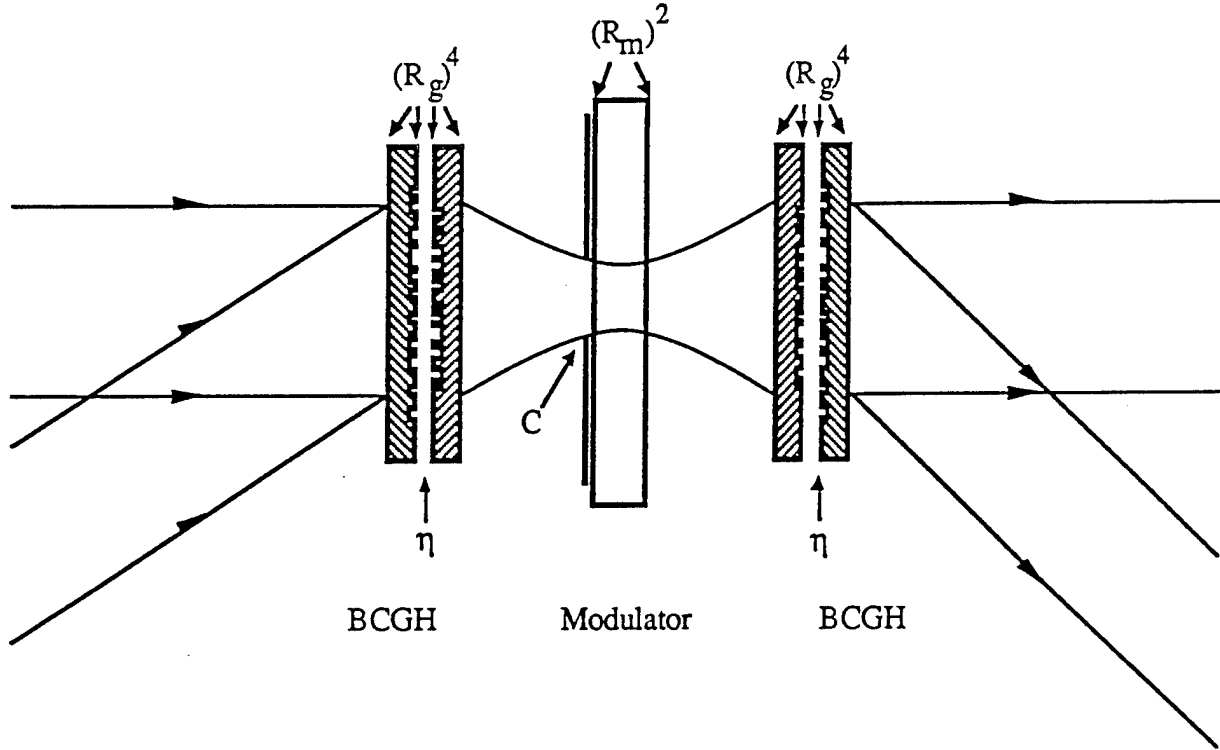


Figure 2: BCGH polarization-based switching element for circuit switched MIN

2.2 Network Control Algorithms

The primary advantage of the BCGH free-space optical MIN over electronic approaches is that the network operates in a fully passive circuit switched mode. That is, once the network state is set, data flows freely through the network without electronic detection and optical signal regeneration. This decouples the data modulation rate from the MIN, making extremely high ($\gg 1$ GHz) data rates possible. The next question is how the network switching state should be controlled. Four distinct types of circuit switching control algorithms can be defined: centralized control with global switching, centralized control with direct injection, centralized control with packet headers, and distributed control with self-routing packet headers. Figure 3 shows each approach schematically.

In centralized control with global switching, the switches in each layer of the network are linked, and can only switch as a unit. The major advantage of this approach is that the switches are simple bulk modulators, rather than pixellated arrays, making the network very easy to construct. However, only a single arbitrary interconnection of one input to one output can be made at one time. Either the interconnections must be multiplexed in time N , or a limited subset of the interconnections used. This method is clearly of little or no interest for most applications. It is useful only as a preliminary

laboratory demonstration step in the development of efficient switches.

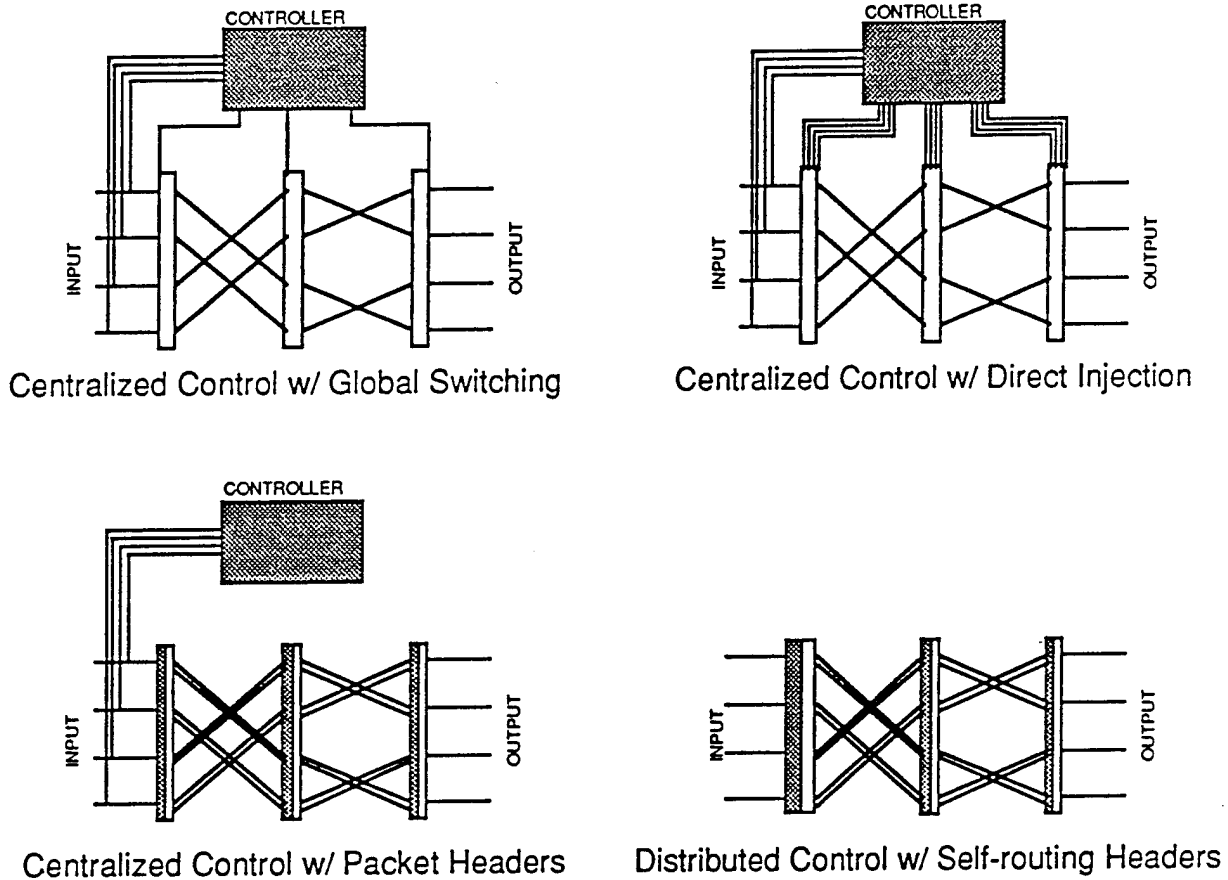


Figure 3: Schematic description of the possible routing control algorithms for MINs

For centralized control with direct injection, the routing algorithm is calculated at a central controller which has direct and independent connections to every switching node (possible through an intermediate memory module which accesses the elements sequentially or in a semi-parallel fashion). This is a way of implementing pure circuit switching, exactly analogous to that done in electronic telecommunications networks. This method is not very scaleable; pin-out problems from the central controller seriously impedes the growth of the network. The time required to load the switch states grows linearly (at least) with N . Parallel optical loading could in principle be used where an external spatial light modulator (SLM) images the switch state information onto the switch array. This merely moves the switch setup problem to the SLM, with no improvement in performance. This approach is therefore useful for BCGH MINs only as an intermediate demonstration step.

Centralized control with packet headers is a more interesting approach for BCGH MINs in that it offers capabilities and characteristics different from any existing MIN. The routing algorithm is performed at a centralized controller, but the process of setting the switches is implemented using

packet headers which propagate through the network. This can be achieved using only a few (<50) transistors per switch and can be achieved using BCGH coupled with smart SLM technology. The routing information must still be distributed to the data source array, but not to the arrays at each layer of the network. The rearrangeably non-blocking MINs discussed in the next section will be amenable to such an implementation. The difference between the existing packet switched networks and the BCGH MIN is that we can perform "virtual" circuit switching by specifying a dedicated header time interval for the packet headers with control information to propagate through the network and set up the required data paths. This will then allow the passive transmission (no detection and rebroadcast costs) at high data rates. The disadvantages of this approach are that it requires synchronous network operation and a more complex ('smart') SLM technology. One main advantage is a reduced controller pin-out (a factor of at least $\log_2 N$ fewer than direct injection). The secondary advantage is that this is an evolutionary step towards the self-routing network as described next.

Distributed control with self-routing packet headers is very promising for BCGH MINs with smart SLMs. This algorithm is typically associated with packet switching, where a short burst of information travels through the network by being received, briefly stored, and rebroadcast at each node. A smart pixel implementation will require about 100 transistors per 1×2 switch.⁵ This approach uses the same smart SLM hardware and interconnection topology as approach (iii). The difference is in the control. Moving the routing to a centralized controller presupposes global interconnection within the controller, albeit at a substantially reduced speed. Here no centralized controller is necessary. This can be a major improvement in cost and scalability. However, the issues of contention and blocking must be addressed either in the hardware (network configuration, size, and switch capability) or software (control and routing algorithms).

The BCGH MIN system for packet header approaches will operate in a synchronous mode. In front of each smart SLM will be a bulk electro-optical modulator whose purpose will be to shift the data stream to an array of detectors controlling the switch states. The modulator is momentarily activated during the point of the header time interval when the address information corresponding to that layer of the network is sent. This way only the part of the packet header needed for that switch will be detected and used. After the header time interval has elapsed the switches will be set according to the packet headers and high-speed passive data transmission can continue. Note that an alternative approach where a fraction of the signal is permanently deflected to the switch detector is inferior for two reasons; (i) more complex electronics at each switch to select the proper data bit, and (ii) unacceptably high power losses for a passive network.

Our conclusion is that competitive photonic circuit switching can be achieved using BCGH technology together with smart SLM technology to implement either centralized control or distributed

control with packet headers. The former is suited to the non-blocking or rearrangeably non-blocking networks (e.g. crossbar, Benes, Dilated Benes, and N-stage) discussed in the following section. The latter approach achieves "virtual-circuit" packet switching (a hybrid between circuit and packet switching) and is well suited to all the networks considered.

2.3 Interconnection Network Topology

We considered several currently existing types of MIN networks: Crossbar, N-Stage Planar, Benes, Dilated Benes, and Batcher Banyon (Figure 4). These networks are representative of MIN networks. The Crossbar and N-Stage networks are locally connected topologies, while the others are globally connected shuffle-type networks. Figure 5, which is one of the graphs found in the architecture design study (appendix A.4), shows the network attenuation vs. the network size for all the topologies considered. The Benes and Dilated Benes had identical good performance, but the added advantage of the Dilated Benes network is suppression of crosstalk noise due to the switch usage. In general we found that the Dilated Benes network made the most effective use of BCGH technology, and therefore it is worth summarizing its characteristics.

The Dilated Benes Network was originally invented for waveguide couplers, which tend to have significant crosstalk.⁶ The Benes network consists basically of two $\log_2 N$ networks placed end to end. The network has $2\log_2 N - 1$ stages, which is the theoretical minimum number of stages required for rearrangeably non-blocking operation. The type of interconnection pattern used can be any binary permutation network, including the butterfly as well as the crossover, shuffle exchange, etc. This is a globally interconnected topology, unlike the crossbar and N-stage networks. The Dilated Benes network is a Benes network which has been doubled in width while maintaining the initial number of inputs and outputs. The first and last layers are 1×2 and 2×1 switches, respectively. The network has the unique advantage that no switching element carries more than one active signal. The full capability of the optical switches, simultaneously carrying signals along two intersecting paths, is not used. In exchange, noise can only get into the signal line by passing through two nominally 'off' switches. If second order crosstalk is negligible (usually true), then the network has a theoretically infinite signal to noise ratio (SNR). Dilated Benes networks have $2\log_2 N$ stages and N switches per stage.

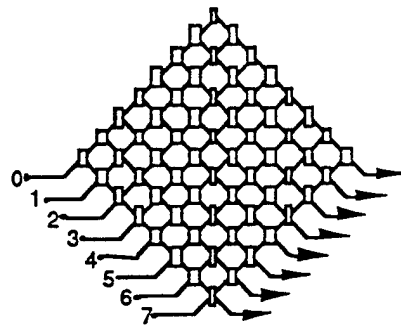
Note that the appendix also includes a table showing the attenuation, SNR, number of stages, the total number of switches, and the maximum network size for each of the architectures considered. Figure 5 and 6 of this final report summarizes the results, showing the network attenuation and SNR, number of stages, and network size achievable with each network. The maximum acceptable attenuation was assumed to be 30 dB (99.9%) and the minimum SNR assumed to be 11 dB, corresponding to a bit error rate (BER) of 10^{-9} .⁷

Our results indicate that certain types of highly connected networks such as crossbars and MINs are not well suited to implementation with BCGH. However, other networks are very well suited to this implementation. The Batcher Banyon MIN scales up to 256x256. Both the Benes and Dilated Benes scale beyond 16Kx16K, making them good choices in terms of attenuation limits. In terms of SNR, when $\beta_s = 30$ dB the Benes network scales beyond 16K. When β_s is lowered to 20 dB, the crosstalk from the switches along the routing paths severely limit the scalability of these networks and a dilated network must be used to counter the effect. Finally in terms of switch count the Benes MIN has the smallest number of switches ($N[2N\log_2 N - 1]/2$). The dilated Benes has roughly twice this number, while both the crossbar and N-stage require $\mathcal{O}(N^2)$ switches.

In summary, we have conducted a study of different architectures for implementation of the multistage interconnection network (MIN). In this study we have considered the technological constraints of the BCGH performances for construction of scaleable MIN. We considered different control algorithms and interconnection network architectures and estimated their performance using BCGH technology in a passive all-optical network. We concluded from this study that Benes network, which is a rearrangeably non-blocking MIN, is well suited to large scale implementations of circuit-switched photonic interconnection networks using BCGH switching elements. The network designed uses packet headers to establish the circuit paths during a dedicated header time interval. The system can use either a centralized controller to determine the appropriate circuit paths or leave the task to the individual input processors to implement a distributed control algorithm. The choice will drive the required smart SLM technology and required pixel complexity or grain size. Finally, the use of a dilated Benes network can alleviate any crosstalk problems that may be characteristic to the pixellated BCGH switch. Most importantly, the size of the network realistically possible using BCGH technology may be as large as 16,384 inputs, well above the size and data modulation rate achievable with all-electronic networks.

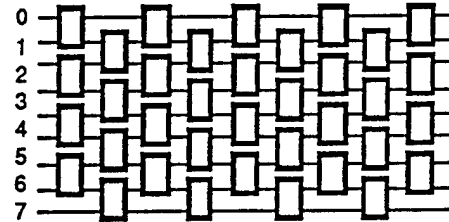
CROSSBAR

N stages,
 N^2 switches



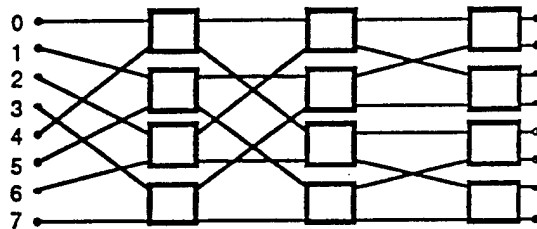
N-STAGE PLANAR

N stages,
 $N(N-1)/2$ switches



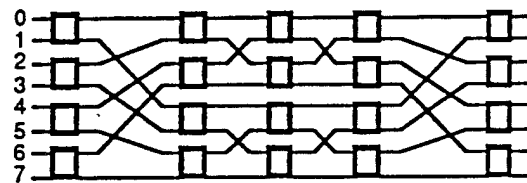
BATCHER-BANYON

$\log_2 N(\log_2 N + 1)/2 + \log_2 N$ stages,
 $N/2 \times (\text{\# of stages})$ switches



BENES (w/ BUTTERFLY)

$2\log_2 N - 1$ stages,
 $N/2 (2\log_2 N - 1)$ switches



DILATED BENES

$2\log_2 N$ stages,
 $2N\log_2 N$ switches

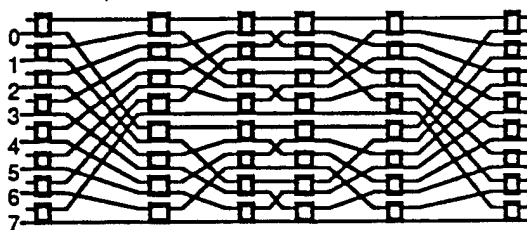


Figure 4: MIN interconnection architectures considered

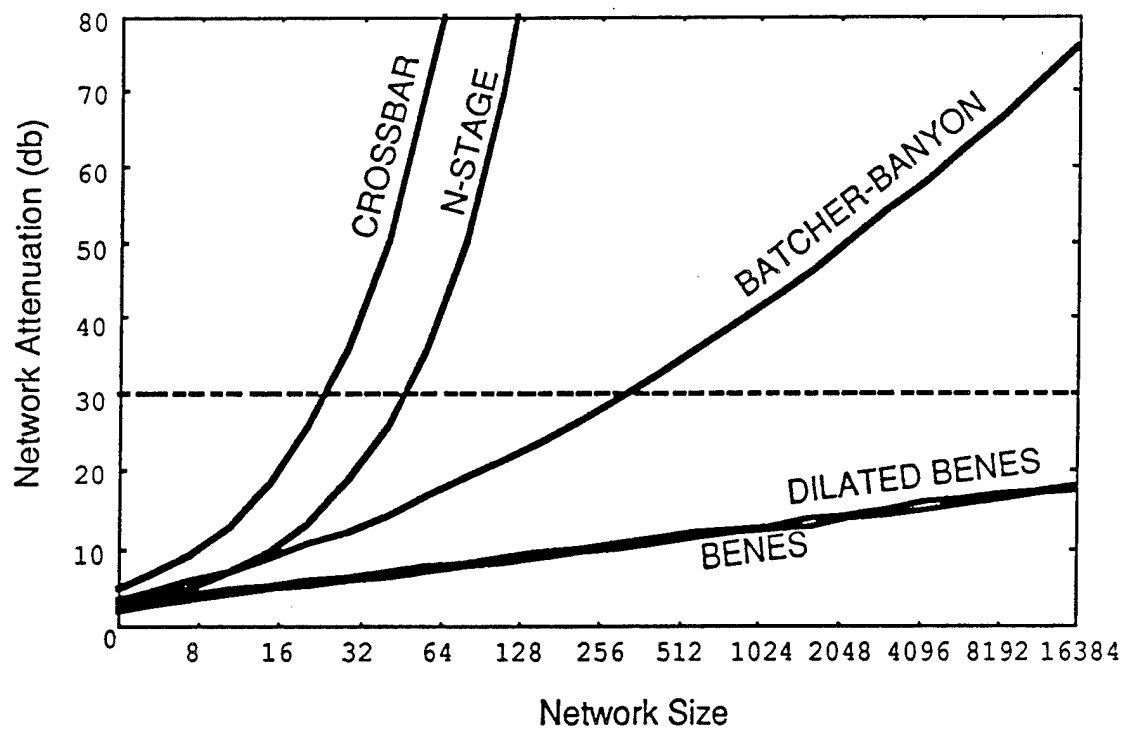


Figure 5: Network attenuation for various network topologies (switch insertion loss -0.64 dB).

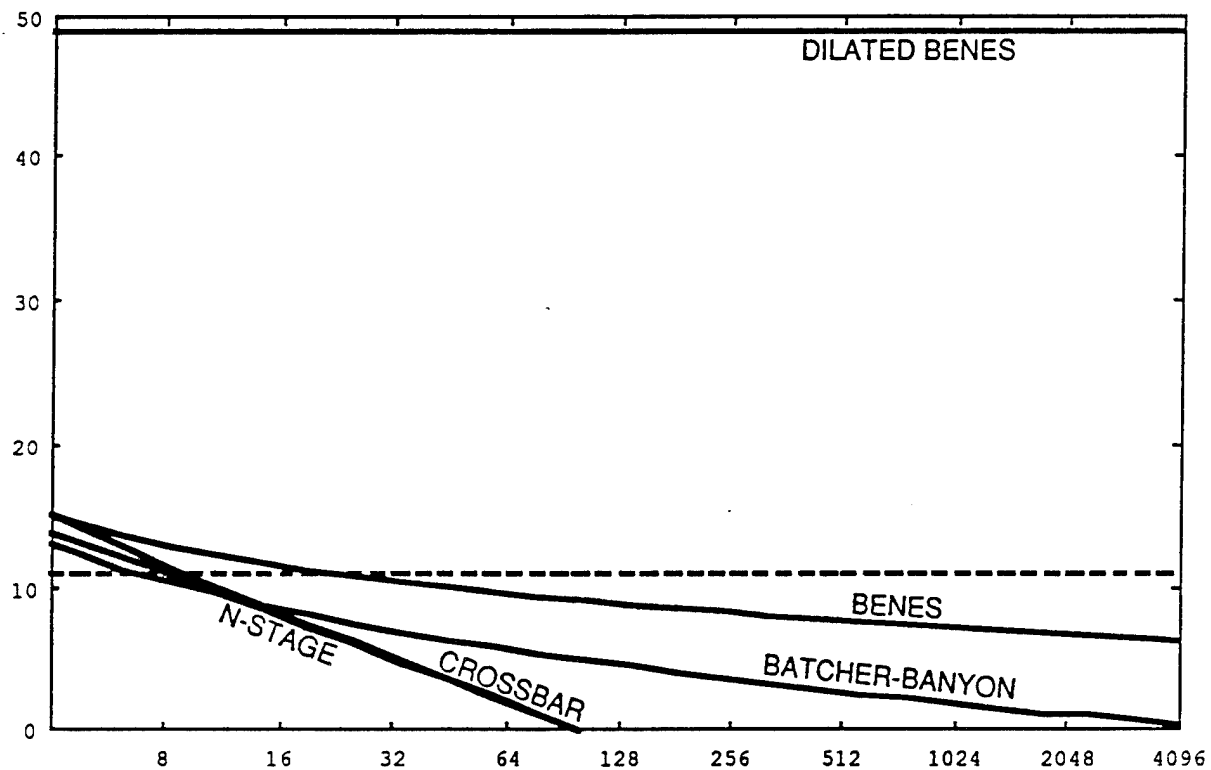


Figure 6: Network SNR in dB vs. network size.

3.1 BCGH Design

The process of BCGH design is described in detail in reference 4. A conventional kinoform CGH is a 2-D phase profile which transforms the input light (e.g., a plane wave) into the desired output (e.g., an array of points). The desired continuous phase profile is first computed, then reduced to a minimum of data by pixellation, truncation to modulo 2π , and quantization into discrete values. This data array is what will actually be fabricated in the hologram.

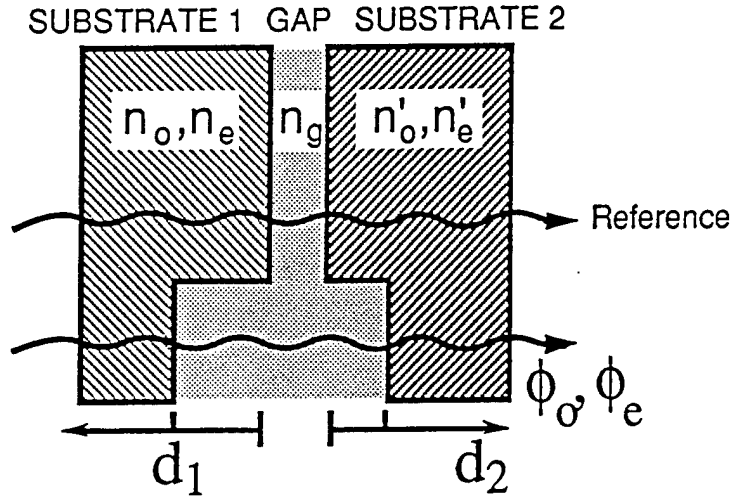


Figure 7: The BCGH is composed of two etched substrates, at least one birefringent, in contact.

In a conventional kinoform, the desired phase values ϕ are obtained by etching the isotropic substrate to a depth proportional to ϕ , where the multiplier is chosen to match the design wavelength λ . A depth $d = \lambda / (n-1)$ corresponds to a full 2π phase difference. The phase patterns are applied lithographically. The F/number of the hologram is determined by the maximum deflection angle, which is a function of the minimum fringe period which can be fabricated according to $F/\# = \frac{1}{2}\sqrt{d^2/\lambda^2 - 1}$. A feature size of $10\mu\text{m}$, for example, corresponds to a fringe period of $20\mu\text{m}$ and produces a F/# of 20 for green light. The number of discrete phase levels fabricated N determines the maximum diffraction efficiency of the hologram η_{max} according to $\eta_{\text{max}} = \text{sinc}^2(1/N)$. The first etch to a depth of π achieves binary phase with an η_{max} of 40.5%, the second etch of an additional $\pi/2$ achieves 4-level phase and increases η_{max} to 81.1%, the third etch of $\pi/4$ achieves 8-level phase and increases η_{max} to 95.0%, and the fourth etch of $\pi/8$ achieves 16-level phase and increases η_{max} to 98.7%. The actual diffraction efficiency is also limited by the transmission through the bulk substrate (absorption and surface reflections) and the accuracy with which the features are fabricated.

The process of fabricating a BCGH is essentially similar, except that the etch depth calculation

involves both ordinary and extraordinary phase values, and the final hologram is assembled from two surface relief etched elements. Figure 7 shows the BCGH geometry, looking at a single pixel of the hologram. Etch depths d_1 and d_2 must be computed so as to create the proper phase delay at each pixel with respect to the reference (unetched portion) for both the ordinary and extraordinary polarizations.

Consider the case of one birefringent and one isotropic substrate, where the polarization of the incident light is either aligned with or perpendicular to the birefringent substrate's optical axis. A ray transmitted through the birefringent substrate will have a different phase delay for each polarization because the index of refraction is different. The phase angle between the two polarizations and the absolute phase delay of the rays depend on the thickness, and hence the etch depth, of the birefringent substrate. This etch depth is chosen to obtain the desired *final phase angle* between the two polarizations. The ray then passes through the isotropic substrate, where light of either polarization is delayed by the same phase angle, again depending on the etch depth. This etch depth is chosen to bring one polarization to the desired phase angle. Since the relative delay between polarizations is unaffected by the isotropic substrate, the phase angle for the orthogonal polarization is simultaneously brought to the final desired value. Because introducing a constant phase is normally not a concern in diffractive optical elements, the substrate thickness does not affect performance.

The etch depths are calculated for the more general case of two birefringent substrates as follows. At each pixel, the optical path difference relative to the unetched region is given by

$$\text{ordinary polarization:} \quad d_1(n_o - n_g) + d_2(n_o' - n_g) = \Phi_o \quad (1a)$$

$$\text{extraordinary polarization:} \quad d_1(n_e - n_g) + d_2(n_e' - n_g) = \Phi_e \quad (1b)$$

where the first and second substrates are etched to depths d_1 and d_2 , respectively, the indices of the first substrate are n_o and n_e , the indices of the second substrate are n_o' and n_e' , and the gap material is assumed to be isotropic with index n_g . Solving these two linear equations in two unknowns yields the required etch depths for any combination of phases:

$$d_1 = \frac{(n_o' - n_g)\Phi_e - (n_e' - n_g)\Phi_o}{(n_e - n_g)(n_o' - n_g) - (n_e' - n_g)(n_o - n_g)} \quad d_2 = \frac{(n_o - n_g)\Phi_e - (n_e - n_g)\Phi_o}{(n_e' - n_g)(n_o - n_g) - (n_e - n_g)(n_o' - n_g)} \quad (2)$$

The positive and negative values produced by these equations are normalized to raise the highest feature to zero depth for each substrate. Consider a binary phase grating fabricated in lithium niobate ($n_o = 2.33$ and $n_e = 2.24$ at $\lambda = 514.5$ nm) with an air gap between substrates ($n_g = 1$). The maximum etch depth using glass as the second substrate ($n_o' = n_e' = 1.6$) is $12 \mu\text{m}$, but if the second substrate is also lithium niobate, only rotated by 90° to reverse the axes ($n_o' = 2.24$ and $n_e' = 2.33$), the maximum

etch depth is reduced to 3 μm . Using twin (identical but orthogonally-oriented) birefringent substrates also simplifies fabrication because both substrates can be patterned and etched together.

The four distinct etch values for a dual binary phase hologram (0, 1.37, 1.47, and 2.84) can be achieved with only two etches because the fourth value is the sum of the second and third (the corresponding features are open for neither, the first, the second, or both etch masks). In general, the number of etches required to fabricate an N-level polarization selective hologram is $4\log_2 N$, exactly four times the minimum number of etches for a simple N-level hologram for a single polarization.⁸ Using twin substrates, the number of pattern and etch steps is halved: $2\log_2 N$. A dual 16-level phase hologram would therefore require only 8 etches. For N-level phase, the maximum depth is nearly twice the maximum binary phase depths given above. However, these etch depths are still consistent with standard fabrication techniques such as ion beam milling, and can be reduced using higher birefringence substrates such as calcite.

These calculations treat both surfaces as lying in the same plane. Ideally, the gap between them should be small enough that a negligible amount of light is diffracted into neighboring pixels. As the distance between elements increases, diffraction efficiency decreases and crosstalk between polarizations occurs. Since the gap is necessarily greater than the etch depth, the maximum allowable spatial frequency is limited. Light propagating along the substrate's optic axes maintains its initial linear polarization. However, the polarization state of light propagating at other angles can become mixed and cause crosstalk. The substrate thickness should therefore be minimized and the birefringence maximized. The most accurate fabrication technique would be to somehow deposit and pattern a thin birefringent layer on an isotropic substrate. This approach is both possible and promising, but is beyond the scope of this one year program.

3.2 BCGH Fabrication

The first BCGH fabricated was a binary phase polarization selective hologram using twin lithium niobate substrates. Lithium niobate was chosen for its moderately high birefringence (0.09 at $\lambda = 514.5$ nm) and its availability at low cost in large (3" diameter) y-cut wafers. A disadvantage of lithium niobate is its high index relative to air, which causes a 16% reflection at each surface even at normal incidence. Total transmission loss through all four surfaces was about 50%.

Four different holograms were made: 1) a simple polarizing beam splitter (PBS), to deflect one polarization and transmit the other, 2) a dual PBS, to deflect one polarization vertically and the other horizontally, 3) a dual cylindrical lens, to focus the two orthogonal polarizations into a vertical or horizontal line, and 4) a dual spherical lens, with a focal length of f and $2f$ for vertically and horizontally polarized light, respectively. Each hologram was 5mm x 5mm, with a design wavelength $\lambda = 514.5$ nm.

The focal lengths ($f = 100$ mm, for F/20) and deflection angles (1.5°) were chosen to produce a grating period of at least $20\text{ }\mu\text{m}$, corresponding to a minimum feature size of $10\text{ }\mu\text{m}$. Kinoform patterns were calculated and converted to binary phase for each polarization. Then the two kinoforms were combined to produce mask patterns for two etches of 1.37 and $1.47\text{ }\mu\text{m}$. Chrome masks were generated by electron-beam lithography and transferred to a photoresist on the substrates by contact print lithography.

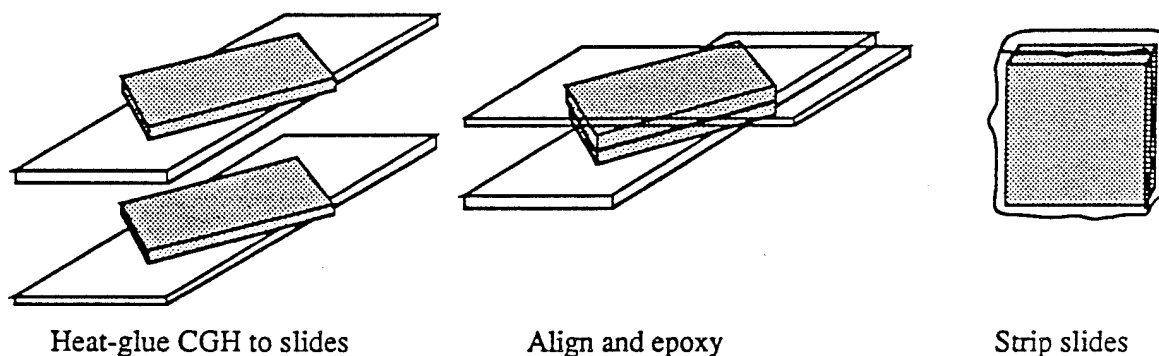
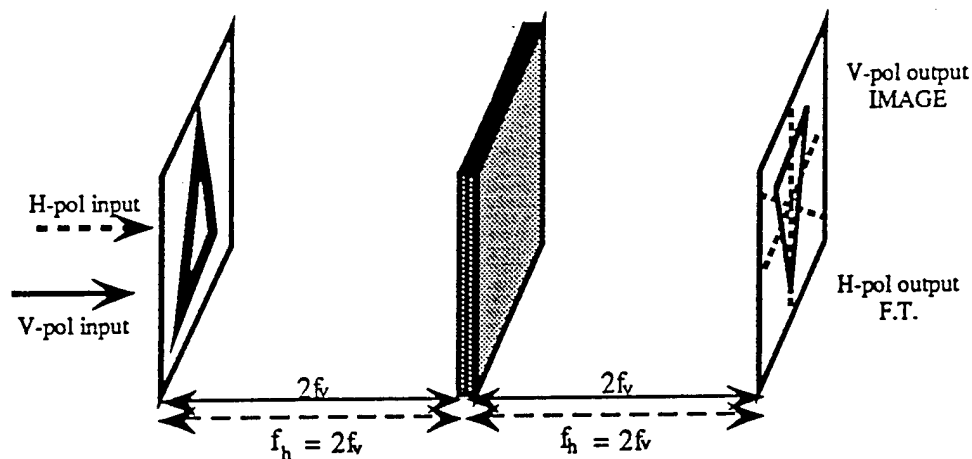


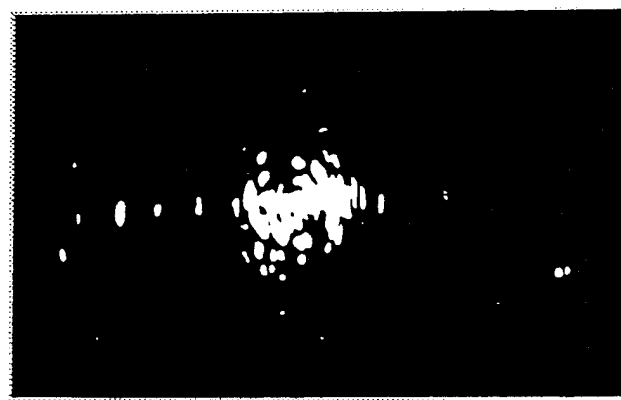
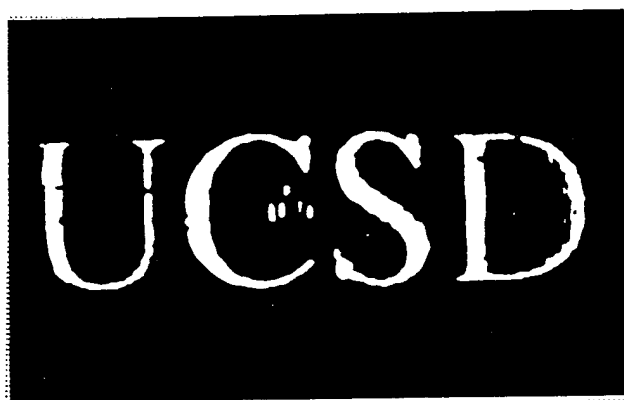
Figure 8: BCGH assembly.

The patterns were etched into the lithium niobate substrate using ion beam milling. The etch depth accuracy measured was $\pm 1\%$. We found that depositing a $0.1\text{ }\mu\text{m}$ layer of chromium between the substrate and the photoresist improved post-etch photoresist removal. (Later, we found that the photoresist could also be removed using a hot nanostrip bath, provided precautions were taken to minimize thermal shock and avoid cracking the substrate). Some lateral etching occurred, producing fringes with sloping side walls and somewhat reduced width ($2\text{ }\mu\text{m}$ per side).

The procedure for BCGH assembly methods is shown schematically in Figure 8. In order to be held by a standard mask aligner, the $25\text{mm} \times 25\text{mm}$ substrates were temporarily mounted to microscope slides with transparent heat-release glue (Aremco Crystalbond 509). The mounted BCGH substrates are placed and roughly aligned in a standard microlithography mask aligner, and then UV curing epoxy (Loctite Chipbond 346) is applied around the edges. After a fine alignment to within an estimated $2\text{ }\mu\text{m}$, the epoxy is cured by UV light, permanently fixing the BCGH substrates together. The assembled BCGH is heat released from the glass slides, and the residue of the heat release glue is removed using acetone. The final product is an apparently monolithic CGH element holding all etched surfaces on the protected interior, allowing standard cleaning as necessary.



(a)



(b)

Figure 9: Experimental arrangement and output for the dual-focus lens.

All of the BCGH were polarization selective as expected. The maximum first order diffraction efficiency η (not including surface reflections) and the polarization contrast ratio R of the four holograms were: for the simple polarizing beam splitter (PBS) $\eta = 25\%$, $R = 10:1$; for the dual polarizing beam splitter $\eta = 6\%$ and $R = 40:1$; for the dual cylindrical lens $\eta = 20\%$ and $R = 6:1$, and for the dual spherical lens $\eta = 17\%$ and $R = 6:1$. Less than 0.2% of the intensity was lost into the zeroth order for the dual PBS, indicating that the proper etch depths were obtained. The theoretical maximum first order efficiency for a binary phase grating is 40%. The low efficiency measured was probably caused primarily by substrate separation and by lateral etching, which changed the duty cycle to up to 2.3:1 in places instead of 1:1.

The dual spherical lens was used to demonstrate a simple optical system which either images or Fourier-transforms the input image depending on the state of the polarization rotator. Figure 9 shows the optical arrangement and photographs of the outputs. Finally, a binary optical switch directing the

output to one of two arbitrary destinations depending on input polarization was demonstrated using the dual polarizing beam splitter. The measured switching contrast ratio was 40:1. This switch was used in the switching node described in Section 4.

3.3 BCGH Performance Improvements

3.3.1 Anti-Reflection Coating

There are two dominant optical losses in a BCGH: surface reflections and hologram diffraction efficiency. While lithium niobate has a high birefringence, it also has a large index of refraction (about 2.3) which causes approximately 16% loss at each of the four surfaces. In addition to reduced transmission efficiency, this can increase background noise and reduce the polarization contrast ratio. To reduce the reflection losses, we had an etched unassembled BCGH substrate coated with a single layer anti-reflection (AR) coating with a silicon dioxide (SiO_2) thin film (of thickness $\lambda/4$ to operate at $\lambda = 514.5 \text{ nm}$) using an ion-plating evaporation system. The reflectance of the AR coated single substrate of lithium niobate was measured to be $0.4 \pm 0.1\%$. Compared to uncoated BCGH, the reflection loss is reduced from 49% to less than 1%. Figure 10 shows the reflectance of lithium niobate substrate with both sides AR coating as a function of wavelength.

3.3.2 In-Situ Alignment

The two separate substrates with the surface relief microstructures must be aligned with high accuracy. The first approach relied on optical inspection of the feature alignment using a standard mask aligner and alignment marks (e.g., cross and diamond pairs). Once the elements are assembled with UV curing epoxy, it is difficult or impossible to separate them again if the alignment turns out to be faulty. An improved method would allow in-situ BCGH testing before curing the epoxy. The principle of the in situ alignment is holding the two lithium niobate substrates in contact with high-precision translation/rotation stages designed to allow illumination of the holograms with a collimated laser beam and real time observation of the resulting diffracted output field using a CCD camera. We maximize the performance of our BCGH element and then apply the UV cured epoxy, cured with hand-held UV light source. This approach was implemented with mixed results. While excellent BCGH performance could be observed before curing the epoxy, performance was not maintained after curing. The apparent source of this problem is shrinkage of the epoxy during curing. This could be cured by being careful to obtain a fully uniform epoxy thickness to equalize stresses, or more simply, by identifying a UV curing epoxy which maintains equal volume during curing.

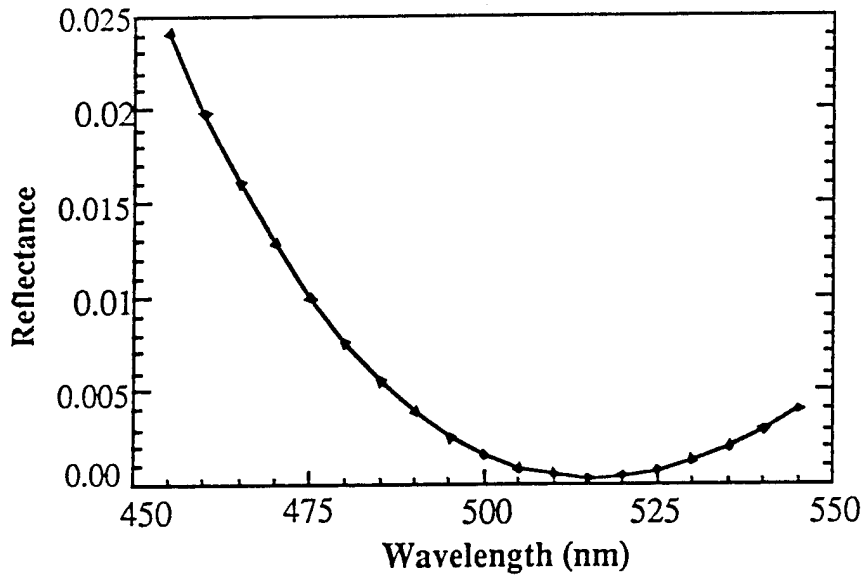


Figure 10: Reflectance of AR coated LiNbO₃ substrate

3.3.3 Multilevel Phase

In general, the maximum theoretical diffraction efficiency achievable by a kinoform CGH is limited by the number of phase levels fabricated. The binary phase BCGH, perfectly fabricated, could achieve a diffraction efficiency of 40.5%, and the best experimentally measured efficiency was 25% for a particular hologram, tilted to the angle which gave the best efficiency. With near normal incidence, the performance was 12% efficiency and a polarization contrast ratio of about 50:1. Diffraction efficiency is also limited by the etch depth and especially feature alignment accuracy. In practice, we found that we could control etch depth accuracy to within approximately $\pm 1\%$, which was sufficiently accurate to have little negative impact on performance. Alignment errors and lateral feature resolution were minimized, but still primarily responsible for the difference between theory and practice.

To increase the diffraction efficiency, we fabricated a multilevel phase (four level) BCGH which doubles the theoretically achievable diffraction efficiency to 80.5%. The BCGH element was designed for application in a multistage interconnection network consisting of 16 nodes, and consisted of a 4x4 array of blazed gratings. The grating periods are 40 μm while the smallest feature size in the hologram is 10 μm which is the same as that used in our binary phase holograms. The performance was increased from a diffraction efficiency of 12% and a polarization contrast ratio of about 50:1 with the binary phase element, to a measured diffraction efficiency of 26.3% and a contrast ratio of 130:1 with the new four-level phase element. More recently, a repeated fabrication of the four-level phase element yielded an increased diffraction efficiency of 60% with a contrast ratio of 160:1. This is the best result

to date.

3.3.4 Future Directions

We have certainly not achieved, or even approached, optimum BCGH performance. In general, we want to achieve diffraction and transmission efficiencies of nearly 100%, while simultaneously reducing the costs of hologram design and fabrication low enough to allow mass fabrication and commercial application. The following is a brief description of some future approaches which might be profitably pursued.

Lithium niobate is not an ideal substrate material. We are examining alternative substrates to improve resolution, diffraction efficiency, and manufacturability. Calcite, while more expensive, has greater birefringence and indices closer to air ($n_o = 1.67$ and $n_e = 1.49$ at $\lambda = 486$ nm). The high birefringence reduces the etch depths, increasing the resolution and maximum diffraction angle, and the low index reduces reflection losses. Stretched polymer materials with moderately high birefringence (0.05) are being manufactured for use as low-cost wave plates. We have successfully etched such materials using reactive ion etching. Polymers could conceivably be patterned by embossing to mass-produce polarization selective holograms at low cost.

It is possible to use a *single* surface-relief etched birefringent substrate to obtain the phases required for both ordinary and extraordinary polarized light by using a multiple order etch depth. We did, in fact, attempt this approach in a preliminary test. However, the etch depths will in general be much higher and the desired phases only approximately matched with this method. A more promising approach is to use form birefringence, where birefringence is created in an isotropic substrate with a grating whose period is much less than the illumination wavelength.⁹ An isotropic glass substrate with a multilevel phase profile can be etched with the high frequency grating to create a variable amount of positive or negative birefringence, depending on the high frequency grating orientation and duty cycle. In this way, the two degrees of freedom necessary to specify both polarization's phase angles are incorporated into the hologram. The feature resolution of such a BCGH could be excellent, and since there is no bulk birefringence, polarization mixing with large beam angles is avoided.

The conclusions which can be drawn from our BCGH fabrication are: 1) the concept has now been proven for both binary and multi-phase level components, 2) the fabrication tolerances have been improved, 3) an improved assembly technique has been developed, and 4) the overall achievable BCGH performance is sufficient to use this element as a component in experimental optical systems. The demonstrated BCGH performance is still less than required for many applications, including the multistage network. Further fabrication improvements are necessary. In particular, the lateral feature resolution and the assembly alignment tolerances must be further reduced to achieve the ultimately

desired performance. However, the measured characteristics lead us to expect that BCGH elements with 98% operating efficiency and 500:1 contrast ratio are only a matter of refinement in the fabrication processes.

4. Sub-System Demonstrations

The original proposal called for the demonstration of a small scale prototype interconnection network using a single polarization modulator per stage. The results of the architecture study described in Section 2 above indicated that emphasis on the BCGH element itself would be more effective in advancing towards ultimate application of the technology. First, it showed that an interconnection network that did not have local switching capabilities would not be useful for any realistic applications. More importantly, it showed that the transmission and diffraction efficiency of the BCGH was the primary factor determining the size of the network which could be constructed. The target BCGH efficiency of 98% and contrast ratio of >100:1 is feasible, but will require substantial development effort. Elements with this performance could be used in networks of more than 1024 nodes, making commercial application of BCGH technology a real possibility. Therefore we chose to emphasize the more fundamental device work over the prototype demonstration. Instead, we made two demonstrations of the switching element itself which allowed us to characterize the switch and make preliminary data transmission measurements.

4.1 1×2 Switch Demonstration

The fabricated BCGH component has been evaluated as a switch in a system environment. The sub-system for this evaluation is shown in Figure 11. A rotating-blade beam chopper is used to modulate an Argon laser (514.5 nm) beam to emulate a single data signal. This modulated signal is then transmitted through a liquid crystal polarization rotator (on loan from Hughes Corporation), which switches the signal polarization at a lower frequency representing the network reconfiguration rate. Upon transmission through the BCGH, depending on the signal polarization, the laser beam is switched between two output photodetectors. Both detectors are connected to the oscilloscope, which displays the signal trace as a function of time.

The experimental results on performance of such a BCGH-based switch are shown in Figure 11. The contrast ratio of the liquid crystal modulator was 200:1, of the BCGH was 40:1, and of the full switch was 25:1.

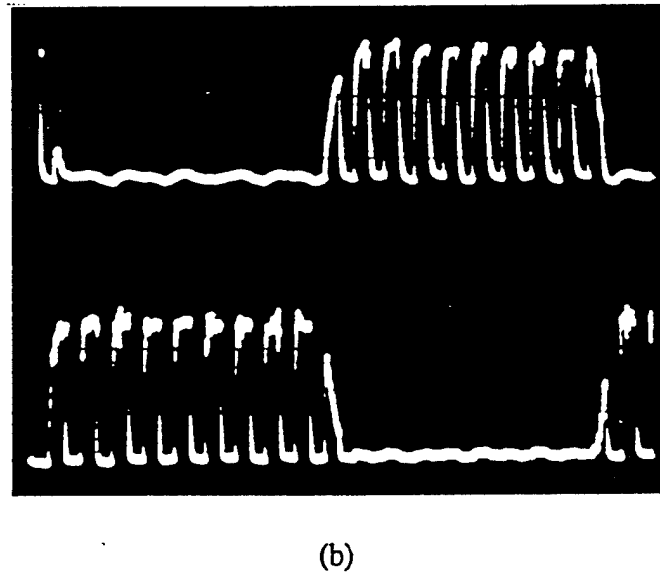
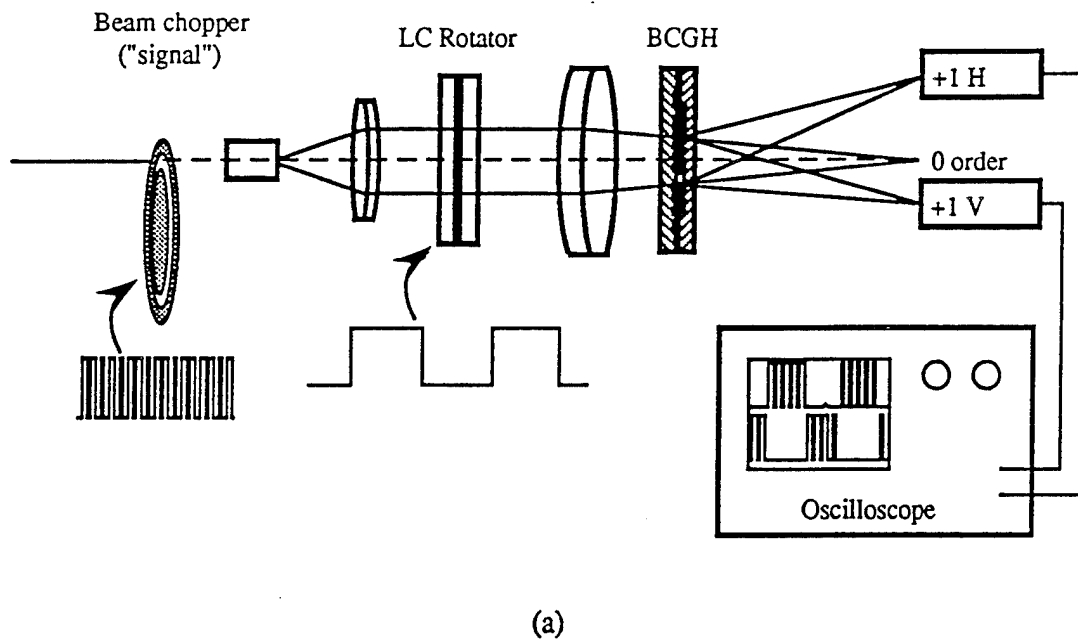
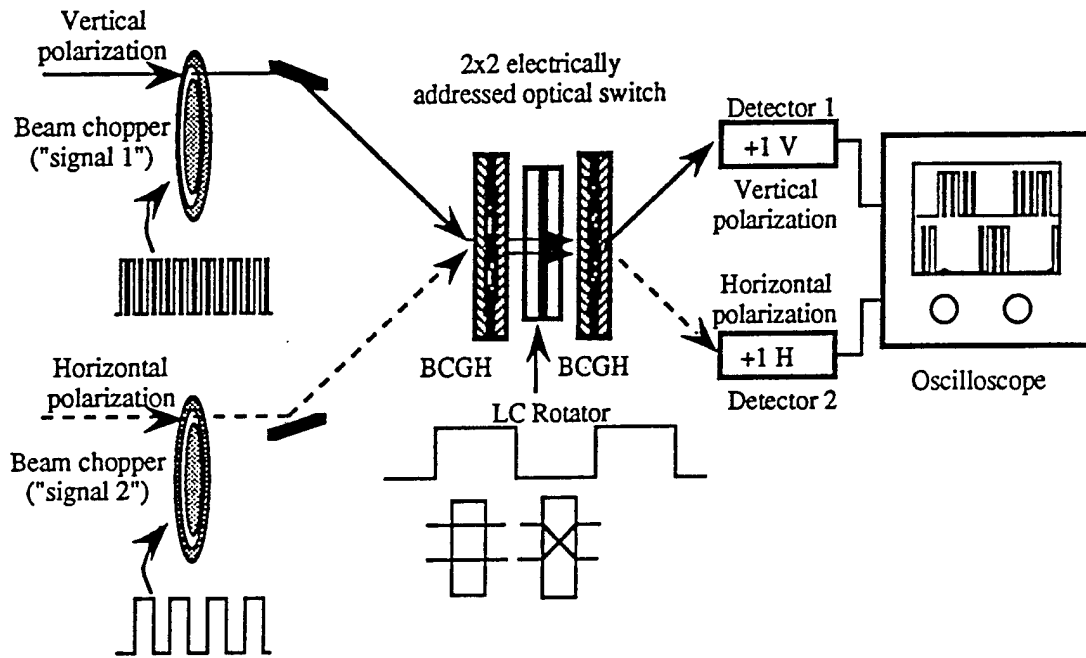


Figure 11: (a) Schematic diagram and (b) oscilloscope trace of the 1x2 BCGH switching node

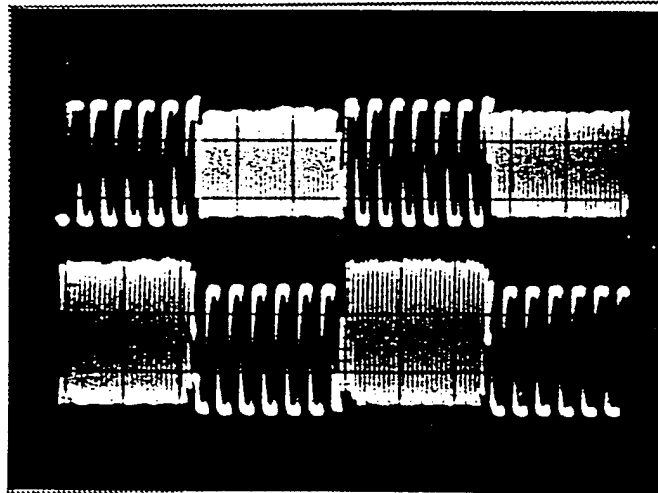
4.2 2 x 2 Switch Demonstration

The fabricated BCGH component has been evaluated for use as a 2x2 switch in a system environment. A 2x2 switch is built from two 1x2 switches. Since a dual BCGH beam splitter (including the focusing function) can be seen as a 1x2 switch, we can construct a 2x2 switch as shown schematically in Fig. 5a. The polarization rotator sandwiched between the two BCGH elements controls the state of the 2x2 switch, i.e., either a cross-over or straight-through connection. The first hologram combines and focuses the two inputs into the modulator, which either exchanges the beam's

polarizations or not. The second hologram separates and directs the outputs to their destinations. Since the optical path is reversible, this element will have same functionality for beams propagating through the optical system in reverse. This allows memory contents to be recalled through the same optical system, along the same optical path, as they were originally stored.



(a)



(b)

Figure 12: (a) Schematic diagram and (b) oscilloscope trace of a 2x2 BCGH switching node

The schematic diagram of our optical setup for demonstration of the 2x2 switch is shown in Figure

12. We simulate two independent information channels for input to the switch by using two beam choppers running at different frequencies to modulate the two orthogonally polarized input beams. The two inputs are both directed into the first BCGH which combines them into the same direction by deflecting the horizontally and vertically polarized light at distinct angles into the same direction. After being combined, the two modulated beams propagate in the same direction through the liquid crystal (LC) polarization rotator. This is essential to obtaining high contrast modulation, as the LC rotator is strongly angle sensitive. After transmission through (and possibly modulation by) the LC rotator, the second BCGH element acts as a dual beam splitter. The beams are deflected into the two different directions depending on their polarization state, and sent into two photodetectors. If the LC is in the off-state the two beams propagate straight through, maintaining their original polarizations and passing through the system as if they had never been combined. But when the LC is turned on, the two beams exchange output detectors. In our experiment we applied a square wave voltage to the LC to cause periodic switching of the light beams between the two output photodetectors. The oscilloscope trace photographs of our experimental results shown at the bottom of Figure 12 demonstrate switching of information between the two channels at the output. The signal to noise ratio (SNR) for a single 1×2 switch was measured as 25:1, and the SNR for the 2×2 switch was comparable.

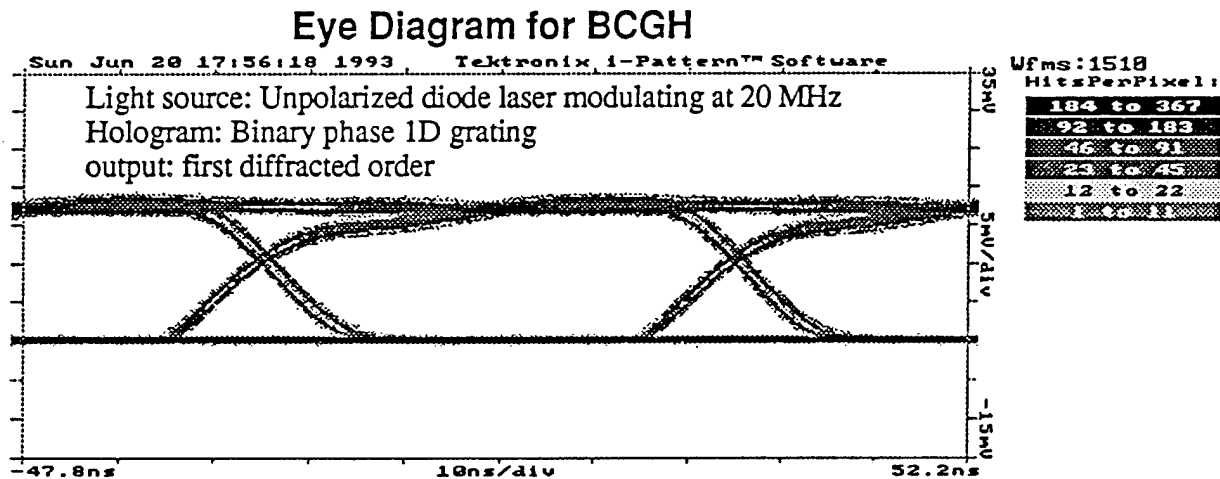


Figure 13: Eye-diagram for 20 MHz data transmission through the BCGH optical switch

The polarization rotator limits the switching speed of the 2×2 switch. In our demonstration, the liquid crystal polarization rotator was operated at a switching rate about 1 KHz. If we use a PLZT or multiple quantum well (MQW)-based polarization rotator, switching as fast as 10MHz to 100MHz can be achieved.

4.3 Fast Data Transmission Demonstration

Once the polarization switch is set, we expect the data transmission rate is determined only by the

speed characteristics of transmitter and receiver. To demonstrate this, we used a diode laser to send a pseudorandom data modulation sequence through the BCGH switch, and measured the diffracted output with a fast oscilloscope to determine how much the data stream quality would be degraded, if at all. We expected that transmission through the switch would have negligible impact on the data contrast ratio, once the switch state was set by the liquid crystal modulator. The eye diagram for data transmitted through the BCGH switch shown in Figure 13 verifies that this is true. Reliable performance for high data rates is possible, limited only by the transmitter speed.

5. Conclusions

5.1 Summary of Accomplishments

The research results of this one year research program can be summarized as follows:

(1) We have demonstrated a unique optical element capable of acting with an arbitrary independent phase function upon illumination with horizontally or vertically polarized monochromatic light. This element, called a BCGH (for birefringent computer generated hologram) is composed of two birefringent substrates, etched with a surface relief patterns and joined face to face. This is a new type of optical element which may be useful in a variety of coherent optical applications, especially when combined with a electro-optic polarization rotator such as a liquid crystal modulator. The application our research was directed towards was a high speed parallel optical interconnection network for memory access.

(2) We have completed a network design study which identified the Dilated Benes network routing algorithm as the most compatible with this technology, and which quantified the importance of BCGH performance in attaining large (≥ 1024 node) networks. We therefore placed more emphasis on achieving high efficiency and contrast ratio BCGH. The diffraction efficiency of the original binary phase LiNbO_3 element was increased from the original result of 6% to 60% by more accurate fabrication and by going to four phase level design, and transmission through uncoated elements was increased from 51% to >99% by antireflection coating. Finally, a contrast ratio between orthogonal polarizations of 160:1 was demonstrated with a diffraction efficiency of 60%.

(3) We have made two subsystem demonstrations using the fabricated BCGH elements. The first was a simple 1×2 polarization switch node which took a single input and directed it into two different outputs depending on polarization. The second was a more complex 2×2 optical node which performed exactly as required for use in passive circuit-switched multistage interconnection networks. It used two BCGH and a liquid crystal polarization rotator to create a switch which combined both routing and switching and allows almost arbitrarily high data modulation rates, with a switching contrast ratio of

better than 50:1. Finally, we used a high speed diode laser source to show 20 MHz data transmission through the switch without significant signal degradation.

From these experimental and theoretical results we conclude that polarization-selective holographic optical elements with transmission and diffraction efficiencies approaching 100% require only fabrication refinements, rather than fundamental design changes. Such elements can become a key component of future optical systems, including a high performance multistage interconnection network for future broadband terabit networks.

5.2 Future Technology Development for Dual Use Applications

The BCGH element apply an arbitrary and independent (computer designed) phase profile to each input polarization. Such phase holograms may have diffraction efficiencies approaching 100%. This capability immediately suggests applications in monochromatic optical systems. For example, as a lightweight readout head for fast access magneto-optic optical disk storage.¹⁰ Even more interesting applications arise when BCGH are combined with active polarization rotating modulators such as electrooptic PLZT¹¹ and liquid crystal¹² modulators. The combination allows direct electrical control of an optical system without introducing moving parts. For example, a "solid state" zoom lens could be designed to switch between multiple discrete positions with a microsecond time response.

The development of polarization-selective CGH elements will continue at UCSD by means of a three year grant from the National Science Foundation. Future device research will involve fabrication of two component BCGH in birefringent substrates that possess low refractive index and high birefringence (e.g., calcite). It will also explore the design and fabrication of high performance *single substrate* BCGHs using more advanced fabrication techniques.

During this project we have demonstrated a new optical component with unique potentials for coherent optical systems. We remain interested in investigating many possible practical dual use applications of this technology. One application is the multistage interconnection network which we have investigated during the past year. Other applications which might be easier to achieve in the near term involve inserting the polarization-selective optical elements in less complex optical systems. For example, as a lightweight and compact readout head for magneto-optic optical disk storage systems. Based on these new experimental results, we anticipate that such opportunities will come to light.

5.3 Acknowledgments

Much of the BCGH element fabrication was performed by two outstanding students involved with this project. The first, Kristopher Urquhart, was instrumental in the first fabrication and has since

graduated with his Ph.D. The second, Fang Xu, is currently continuing research on polarization-selective CGH at UCSD.

6. References

- 1 J. E. Ford, F. Xu, K. Urquhart, and Y. Fainman, "Polarization selective computer generated holograms," Post deadline Paper, OSA Annual Meeting, Albuquerque, September 1992. (1/2 page)
- 2 J. E. Ford, F. Xu, K. Urquhart, and Y. Fainman, "Polarization selective computer generated holograms," *Opt. Lett.* **18**, p.456-458, 1992.
- 3 J. Ford, F. Xu, A. Krishnamoorthy, K. Urquhart, and Y. Fainman, "Polarization-selective computer generated holograms for optical multistage interconnection networks," OSA Topical Meeting on Optical Computing, Tech. Dig. Series Vol. 7, 258-261, Palm Springs CA, March 1993.
- 4 F. Xu, J. Ford, and Y. Fainman, "Polarization selective computer generated holograms and applications," SPIE Intl. Symp. on Optics, Imaging, and Instrumentation, Paper 1992-19, San Diego, CA July 1993.
- 5 A. Krishnamoorthy, P. Marchand, F. Kiamilev, and S. Esener, "Grain-size considerations for optoelectronic multistage interconnection networks," *Applied Optics* **31**, 5480-5507, 1992.
- 6 K. Padmanaphan and AZ. Netraveli, "Dilated networks for photonic switching," *IEEE Transactions on Communications* **C-30**(12), December 1987.
- 7 Ailawadi, "Photonic switching architectures and their comparison," in Frontiers in Computing Systems Research, Vol. 1, S. Tewksbury Ed., Plenum Press 1990.
- 8 G. Swanson, "Binary Optics Technology: The Theory and Design of Multi-level Diffractive Optical Elements". M.I.T. Lincoln Laboratory Tech. Rep. 854, August 1989.
- 9 D. C. Flanders, "Submicrometer periodicity gratings as artificial anisotropic dielectrics", *Appl. Phys. Lett.* **42**, 492-494, 1983.
- 10 A. Ohba, Y. Kimura, S. Sugama, R. Katayama, and Y. Ono, "Reflection polarizing holographic optical element for compact magneto-optical disk heads," *Appl. Opt.* **29**, 5131-5135, 1990.
- 11 C. J. Kirkby, M. J. Goodwin, A. D. Parsons, "PLZT/silicon hybridized spatial light modulator array - design, fabrication and characterization," *Intl. J. of Optoelectronics* **5**, 169-178, 1990.
- 12 L. K. Cotter, T. J. Drabik, R. J. Dillon and M. A. Handschy, "Ferroelectric-liquid-crystal/silicon-integrated-circuit spatial light modulator," *Opt. Lett.* **15**, 291-293, 1990.

Appendices

Appendix 1

Polarization-selective computer-generated holograms

J. Ford, F. Xu, K. Urquhart and Y. Fainman

Optics Letters, Vol. 18, No. 6, 456-458, March 1993

Polarization-selective computer-generated holograms

Joseph E. Ford, Fang Xu, Kristopher Urquhart, and Yeshaiah Fainman

Department of Electrical and Computer Engineering, University of California, San Diego, La Jolla, California 92093-0407

Received September 22, 1992

We demonstrate polarization-selective computer-generated holograms with independent phase profiles for the two orthogonal linear polarizations. The holograms are made of two surface-relief-etched birefringent substrates joined face to face. We describe their design and fabrication and present experimental results for dual binary-phase computer-generated holograms fabricated in lithium niobate. The first-order diffraction efficiency varied from 6% to 25%, with as much as 40:1 contrast between polarizations. Such elements can be used in compact optoelectronic systems or combined with electro-optic polarization rotators to make electrically controlled optical elements.

Computer-generated holograms (CGH's) fabricated as phase-only optical elements have proven useful for aberration correction, lenslet arrays, interconnection, and other applications. Such elements are normally insensitive to input light polarization, but a polarization-selective CGH would be useful. A compact optoelectronic system that uses modulator arrays might incorporate an element that generates a spot array from an off-axis vertically polarized optical power beam and then deflects and focuses each horizontally polarized output to its destination. This element would replace at least two conventional CGH's and a polarizing beam splitter. Alternatively, polarization-selective CGH could be combined with liquid-crystal polarization rotators to make electrically controlled monochromatic optical systems. A stepping zoom lens could be made with microsecond response and no moving parts.

Polarization-selective holographic optical elements have been optically recorded in organic dyes,¹ photorefractive crystals,² and dichromatic gelatin.³ However, optically recorded elements lack the flexibility of planar CGH in realizing an arbitrary phase function. Diffraction-grating polarizing beam splitters have been fabricated by using high-spatial-frequency gratings.⁴ Our physical approach is related to that of Ohba *et al.*,⁵ where proton exchange in lithium niobate was used to create a birefringent grating. However, we use substrate birefringence to construct CGH's with arbitrary diffractive functionality for the two orthogonal linear polarizations.

A conventional-phase CGH can be fabricated by etching an isotropic substrate with a surface-relief pattern that will impose the desired phase delay on an incident optical wave front. To build an optical element with arbitrary function for each of the two orthogonal polarizations, we need to apply an independent phase delay for each polarization at each pixel. This additional information must be physically encoded into the substrate. We use two substrates, with their etched surfaces in contact, to hold this information (see Fig. 1).

Consider the case of one birefringent and one isotropic substrate, where the polarization of the incident light is either aligned with or perpendicular

to the birefringent substrate's optic axis. A ray transmitted through the birefringent substrate will have a different phase delay for each polarization. The phase angle between the two polarizations and the absolute phase delay of the rays depends on the thickness, and hence the etch depth, of the birefringent substrate. This etch depth is chosen to obtain the desired final phase angle between the two polarizations. The ray then passes through the isotropic substrate, where light of either polarization is delayed by the same phase angle, again depending on the etch depth. This etch depth is chosen to bring one polarization to the desired phase angle. Since the relative delay between polarizations is unaffected by the isotropic substrate, the phase angle for the orthogonal polarization is simultaneously brought to the final desired value. Because introducing a constant phase is normally not a concern in diffractive optical elements, the substrate thickness does not affect performance.

The etch depths are calculated for the more general case of two birefringent substrates as follows. At each pixel, the optical path difference relative to the unetched region (see Fig. 2) is given by

ordinary polarization:

$$d_1(n_o - n_e) + d_2(n_o' - n_e) = \Phi_o, \quad (1a)$$

extraordinary polarization:

$$d_1(n_e - n_e) + d_2(n_e' - n_e) = \Phi_e, \quad (1b)$$

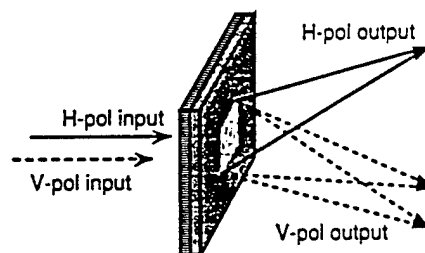


Fig. 1. BCGH geometry, showing the two etched substrates joined face to face. H-pol and V-pol, horizontally and vertically polarized, respectively.

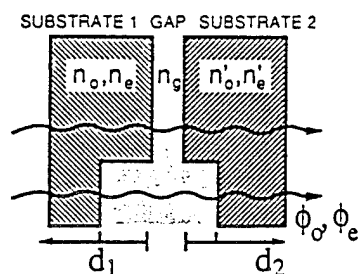


Fig. 2. BCGH construction, showing a single pixel of the hologram.

where the first and second substrates are etched to depths d_1 and d_2 , respectively, the indices of the first substrate are n_o and n_e , the indices of the second substrate are n'_o and n'_e , and the gap material is assumed to be isotropic with index n_g . Solving these two linear equations in two unknowns yields the required etch depths for any combination of phases:

$$d_1 = \frac{(n'_o - n_g)\Phi_e - (n'_e - n_g)\Phi_o}{(n_e - n_g)(n'_o - n_g) - (n'_e - n_g)(n_o - n_g)},$$

$$d_2 = \frac{(n_o - n_g)\Phi_e - (n_e - n_g)\Phi_o}{(n'_e - n_g)(n_o - n_g) - (n_e - n_g)(n'_o - n_g)}. \quad (2)$$

The positive and negative values produced by these equations are normalized to raise the highest feature to zero for each substrate. Consider a binary-phase grating fabricated in lithium niobate ($n_o = 2.33$ and $n_e = 2.24$ at $\lambda = 514.5$ nm) with an air gap between substrates ($n_g = 1$). Table 1 shows the etch depths, using as the second substrate (i) glass ($n'_o = n'_e = 1.6$) and (ii) lithium niobate rotated by 90° to reverse the axes ($n'_o = 2.24$ and $n'_e = 2.33$). The use of identical orthogonally oriented birefringent substrates has two advantages. First, it reduces the absolute value of the etch depths (in this case, from 12 to $3 \mu\text{m}$). Second, fabrication is simplified because both substrates can be patterned and etched together.

The four distinct etch values for a dual binary-phase hologram (0, 1.37, 1.47, and 2.84) can be achieved with only two etches because the fourth value is the sum of the second and third. In general, the number of etches required to fabricate an N -level polarization-selective hologram is $2\log_2 N$, exactly twice the minimum number of etches for a simple N -level hologram for a single polarization.⁶ A dual 16-level phase hologram would therefore require only eight etches. For an N -level phase, the maximum depth is nearly twice the maximum binary-phase depths shown in Table 1. The required etch depths are consistent with fabrication techniques such as ion-beam milling and can be reduced using higher birefringence substrates.

These calculations treat both surfaces as lying in the same plane. Ideally, the gap between them should be small enough that a negligible amount of light is diffracted into neighboring pixels. As the distance between elements increases, diffraction efficiency decreases, and cross talk between polarizations occurs. Since the gap is necessarily

greater than the etch depth, the maximum allowable spatial frequency is limited. Light propagating along the substrate's optic axes maintains its initial linear polarization. However, the polarization state of light propagating at other angles can become mixed and cause cross talk. The substrate thickness should therefore be minimized and the birefringence maximized.

A binary-phase polarization-selective hologram was fabricated by using two orthogonally oriented lithium niobate substrates. Lithium niobate was chosen for its moderately high birefringence (0.09 at $\lambda = 514.5$ nm) and its availability at low cost in large [3-in.- (7.6-cm) diameter] y-cut wafers. A disadvantage of lithium niobate is its high index relative to air, which causes a 16% reflection at each surface even at normal incidence. Total transmission loss through all four surfaces was over 50%.

Four different holograms were made: (1) a simple polarizing beam splitter (PBS), to deflect one polarization and transmit the other; (2) a dual PBS, to deflect one polarization vertically and the other horizontally; (3) a dual cylindrical lens, to focus the two orthogonal polarizations into a vertical or horizontal line; and (4) a dual spherical lens, with a focal length of f and $2f$ for vertically and horizontally polarized light, respectively. Each hologram was $5 \text{ mm} \times 5 \text{ mm}$, with a design wavelength $\lambda = 514.5$ nm. The focal lengths ($f = 100$ mm, for $F/20$) and deflection angles (1.5°) were chosen to produce a grating period of at least $20 \mu\text{m}$, corresponding to a minimum feature size of $10 \mu\text{m}$. Kinoform patterns were calculated and converted to binary phase for each polarization. Then the two kinoforms were combined as in Table 1 to produce mask patterns for two etches of 1.37 and $1.47 \mu\text{m}$. Chrome masks were generated by electron-beam lithography and transferred to a photoresist on the substrates by contact print lithography.

The patterns were etched into the lithium niobate substrate by using ion-beam milling. The etch-depth accuracy measured was $\pm 1\%$. We found that depositing a $0.1\text{-}\mu\text{m}$ layer of chromium between the substrate and the photoresist improved postetch photoresist removal. Some lateral etching occurred, producing fringes with sloping side walls and somewhat reduced width ($2 \mu\text{m}$ per side). In order to be held by a standard mask aligner, the $25 \text{ mm} \times 25 \text{ mm}$ substrates were temporarily fixed to microscope

Table 1. Etch Depths Required for Binary-Phase Polarization-Selective Holograms^a

Phases		Lithium Niobate and Glass		Both Lithium Niobate	
Φ_o	Φ_e	d_1	d_2	d_1	d_2
0	0	2.85	5.89	1.37	1.37
$\lambda/2$	0	0	12.21	0	2.84
0	$\lambda/2$	5.70	0	2.84	0
$\lambda/2$	$\lambda/2$	2.85	6.32	1.47	1.47

^aAll etch depths in micrometers, with $\lambda = 514.5$ nm.

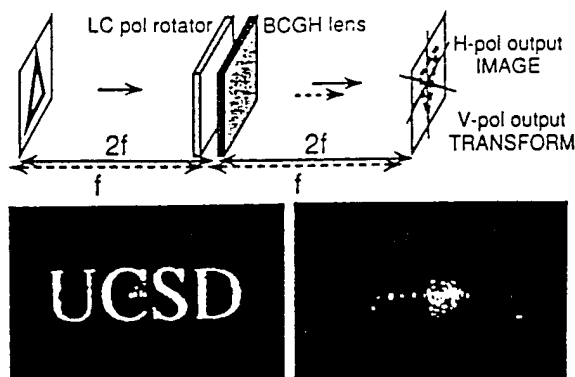


Fig. 3. Experimental arrangement and output for simple electrically controlled optical system that either images (left-hand side) or Fourier transforms (right-hand side) the input plane depending on the voltage applied to a liquid-crystal (LC) polarization rotator.

slides with transparent heat-release glue (Aremco Crystalbond 509). The substrates were aligned to within an estimated $2\ \mu\text{m}$, then permanently joined with UV-curing epoxy (Loctite 346) around the edges. Finally, the microscope slides were removed, yielding an apparently monolithic hologram with the features on the interior surfaces.

All the birefringent CGH's (BCGH's) were polarization selective as expected. The maximum first-order diffraction efficiency η (not including surface reflections) and the polarization contrast ratio R of the four holograms were as follows: for the simple PBS, $\eta = 25\%$ and $R = 10:1$; for the dual PBS, $\eta = 6\%$ and $R = 40:1$; for the dual cylindrical lens, $\eta = 20\%$ and $R = 6:1$; and for the dual spherical lens, $\eta = 17\%$ and $R = 6:1$. Less than 0.2% of the intensity was lost into the zeroth order for the dual PBS, indicating that the proper etch depths were obtained. The theoretical maximum first-order efficiency for a binary-phase grating is 40%. The low efficiency measured was probably caused primarily by substrate separation and by lateral etching, which changed the duty cycle to as high as 2.3:1 in places, instead of 1:1.

The dual spherical lens was used to demonstrate a simple electrically controlled optical system that either images or Fourier transforms the input image depending on the voltage applied to a liquid-crystal polarization rotator (see Fig. 3). Finally, a binary optical switch that directed the output to one of two arbitrary destinations depending on input polarization was demonstrated by using the dual PBS. The measured switching contrast ratio was 40:1. This switch is currently being used to construct a circuit-switched optical interconnection network.

Lithium niobate is not an ideal substrate material. Calcite, though more expensive, has greater birefringence and indices closer to air ($n_o = 1.67$ and $n_e = 1.49$ at $\lambda = 486\ \text{nm}$). The high birefringence reduces the etch depths, thereby increasing the resolution and maximum diffraction angle, and the low index reduces reflection losses. Stretched polymer materials with moderately high birefringence

(0.05) are being manufactured for use as low-cost wave plates. We have successfully ion etched such materials and are currently fabricating the same binary-phase BCGH's with them. Polymers could conceivably be patterned by embossing in order to mass produce polarization-selective holograms at low cost.

It is possible to use a single surface-relief-etched birefringent substrate to obtain the phases required for both ordinary and extraordinary polarized light by using a multiple-order etch depth. However, the etch depths will be much higher and the desired phases only approximately matched with this method. A more promising approach is to use form birefringence, where birefringence is created in an isotropic substrate with a grating whose period is much less than the illumination wavelength.⁷ An isotropic glass substrate with a multilevel phase profile can be etched with the high-frequency grating to create a variable amount of positive or negative birefringence, depending on the high-frequency grating orientation and duty cycle. In this way, the two degrees of freedom necessary to specify both polarizations' phase angles are incorporated into the hologram. The feature resolution of such a BCGH could be excellent, and since there is no bulk birefringence, polarization mixing with large beam angles is avoided.

In conclusion, we have introduced a method for constructing a polarization-selective CGH by using surface-relief etching of birefringent substrates. We have demonstrated this approach by using two orthogonally oriented lithium niobate substrates in contact. Four binary-phase holograms were tested, producing diffraction efficiencies from 6% to 25%, with a contrast ratio between polarizations of as high as 40:1. Finally, we have suggested alternative constructions of the birefringent CGH, including one that can be fabricated in a single isotropic substrate by using form birefringence.

The authors thank Hughes Aircraft for its loan of a liquid-crystal polarization rotator. We also thank Sadik Esener, Sing Lee, Chi Fan, Walter Däshner, Jinghua Wang, Brian Catanzaro, and Subramania Krishnakumar for their valuable contributions. This research was funded by the U.S. Air Force Rome Laboratory under grant F-30602-91-C-0094.

References

1. T. Todorov, L. Nikolova, K. Stoyanova, and N. Tomova, *Appl. Opt.* **24**, 785 (1985).
2. Q. W. Song, M. C. Lee, P. J. Talbot, and E. Tam, *Opt. Lett.* **16**, 1223 (1991).
3. R. Kostuk, M. Kato, and Y. T. Huang, *Appl. Opt.* **29**, 3848 (1990).
4. A. Ohba, Y. Kimura, S. Sugama, R. Katayama, and Y. Ono, *Appl. Phys.* **29**, 5131 (1990).
5. A. Ohba, Y. Kimura, S. Sugama, Y. Urino, and Y. Ono, *Jpn. J. Appl. Phys.* **28** (Suppl. 28-3), 359 (1989).
6. G. Swanson, M.I.T. Lincoln Lab. Tech. Rep. 854 (August 1989).
7. D. C. Flanders, *Appl. Phys. Lett.* **42**, 492 (1983).

Appendix 2

Polarization-selective computer-generated holograms for optical multistage interconnection networks

J. Ford, F. Xu, A. Krishnamoorthy, K. Urquhart and Y. Fainman

OSA Topical Meeting on Optical Computing, Technical. Digest. Series Vol. 7, 258-261
Palm Springs CA, March 1993.

Polarization-Selective Computer-Generated Holograms for Optical Multistage Interconnection Networks

Joseph Ford, Fang Xu, Ashok Krishnamoorthy, Kristopher Urquhart and Yeshayahu Fainman
University of California San Diego, ECE Dept., La Jolla CA 92093-0407; (619) 534-8909

1. Introduction

Computer-generated holograms (CGH) fabricated as phase-only optical elements have proven to be useful in implementing free space optical interconnections for parallel computing and communications. Such elements are normally capable of implementing a single fixed optical interconnect. The performance of such systems could be enhanced with switching optical interconnects that do not require signal detection and regeneration. A polarization-selective CGH with independent impulse responses for the two orthogonal linear polarizations would introduce an additional degree of freedom useful in designing such systems. An array of such polarization-selective CGH could be combined with electro-optic polarization rotators to build an electrically-controlled optical switch array for implementing a passive multistage interconnection network (MIN) supporting fast data transmission bandwidths.

Optically recorded polarization-selective holographic optical elements have been obtained using various media. However, CGH offer possible advantages over optically recorded elements in efficiency, repeatability, and generality. Our goal is a polarization selective CGH. Our physical approach is related to that of Ohba et al,¹ where proton exchange in lithium niobate was used to create a birefringent grating compensated by a surface dielectric layer. This approach produces a single hologram, invisible to the orthogonal polarization. In contrast, our approach² yields CGH with arbitrary functionality for each of the two orthogonal linear polarizations.

2. Design and fabrication of the birefringent CGH

A conventional phase CGH can be fabricated by etching an isotropic substrate with a surface relief pattern which will impose the desired phase delay on an incident optical wavefront. To build an optical element with arbitrary function for each of the two orthogonal polarizations, we need to apply an independent phase delay for each polarization at each pixel. This additional information must be physically encoded into the substrate. We use two birefringent substrates, with their etched surfaces in contact, to hold this information (see Figure 1).

These two substrates can apply an arbitrary phase for the two orthogonal linear polarizations of a transmitted light ray. Consider the case of one birefringent and one isotropic substrate, where the

polarization of the incident light is either aligned with or perpendicular to the birefringent substrate's optical axis. A ray transmitted through the birefringent substrate will have a different phase delay for each polarization because the index of refraction is different. The phase angle between the two polarizations and the absolute phase delay of the rays depends on the thickness, and hence the etch depth, of the birefringent substrate. This etch depth is chosen to obtain the desired final phase angle between the two polarizations. The ray then passes through the isotropic substrate, where light of either polarization is delayed by the same phase angle, again depending on the etch depth. This etch depth is chosen to bring one polarization to the desired phase angle. Since the relative delay between polarizations is unaffected by the isotropic substrate, the phase angle of the orthogonal polarization is simultaneously brought to the final desired value.

The etch depths are calculated for the more general case of two birefringent substrates as follows. At each pixel, the optical path difference relative to the unetched region is given by $\Phi_o = d_1(n_g - n_o) + d_2(n_g - n_o')$ for ordinary polarization and $\Phi_e = d_1(n_g - n_e) + d_2(n_g - n_e')$ for extraordinary polarization, where the etch depths are d_1 and d_2 for the first and second substrates, the indexes of the first substrate are n_o and n_e , the indexes of the second substrate are n_o' and n_e' , and the gap material is assumed to be isotropic with index n_g (see Figure 1). Solving these two linear equations in two unknowns yields the required etch depths for any combination of phases:

$$d_1 = \frac{(n_o' - n_g)\Phi_o - (n_e' - n_g)\Phi_e}{(n_e - n_g)(n_o' - n_g) - (n_e' - n_g)(n_o - n_g)} \quad d_2 = \frac{(n_o - n_g)\Phi_o - (n_e - n_g)\Phi_e}{(n_e' - n_g)(n_o - n_g) - (n_e - n_g)(n_o' - n_g)} \quad (1)$$

The positive and negative values produced by these equations can be normalized to raise the highest feature to zero depth. We designed a binary phase hologram fabricated in lithium niobate ($n_o = 2.33$ and $n_e = 2.24$ at $\lambda = 514.5$ nm), using identical perpendicularly-oriented birefringent substrates. Such an arrangement reduces the etch depths (in this case, from 12 μm to 3 μm) and allows the two substrates to be etched simultaneously. There are four distinct etch values for the hologram (0, 1.37, 1.47, and 2.84) but they can be achieved with only two etches, because the fourth value is the sum of the second and the third. In general, with symmetric substrates the number of etches required to fabricate an N-level polarization-selective hologram is $2\log_2 N$, exactly twice the minimum number of etches with a simple N-level hologram for a single polarization.³

3. Demonstration of the 1x2 switch for multistage interconnection networks

These BCGH elements can be used to construct a self-routing 2x2 binary switch for free space optical interconnections. The switch consists of two dual polarization selective holograms separated by a polarization rotator. Two input beams are combined and possibly focused into the polarization rotator, then separated and redirected by the second dual hologram. The polarization rotator either exchanges

the two beams, or not, depending on the applied voltage. A network constructed of such switches would be circuit-switched, since optical information is routed without detection and signal regeneration. The data modulation rate is limited only by the input sources and output detectors, not by the network itself. However, the switches need to be efficient to preserve signal intensity.

We designed a dual beamsplitter to deflect one polarization vertically and the other horizontally. The hologram was 5mm x 5mm, with a design wavelength $\lambda = 514.5$ nm and a minimum feature size of 10 μm . Kinoform patterns were calculated and converted to binary phase for each polarization. Then the two kinoforms were combined to produce mask patterns for two etches of 1.37 and 1.47 μm . Chrome masks were generated by electron-beam lithography and transferred to a photoresist on the substrates by contact print lithography. The patterns were etched into the lithium niobate substrate using ion beam milling. The accuracy of the etch depth was approximately $\pm 1\%$. Some lateral etching occurred, producing fringes with sloping sidewalls and somewhat reduced width (2 μm per side). The substrates were aligned in a standard mask aligner to within 2 μm , then permanently joined with UV curing epoxy. The maximum first order diffraction efficiency (not including surface reflections) and the polarization contrast ratio of the dual beamsplitter were measured to be 6% and 40:1 respectively. Less than 0.2% of the intensity was lost into the zeroth order.

This element was used in the 1x2 optical switch configuration shown in Figure 2. A beam chopper modulated a laser beam to emulate a data signal. This signal was then transmitted through a liquid crystal polarization rotator, which switched the signal polarization at a lower frequency representing the network reconfiguration rate. Upon transmission through the BCGH, depending on the signal polarization, the modulated laser beam was switched between two output photodetectors. The output of the two detectors is shown in the inset photograph. The contrast ratio of the liquid crystal modulator was 200:1, of the BCGH was 40:1, and of the full switch was 25:1. The efficiency of this switch was limited to 3% due to fabrication errors, but the theoretical hologram efficiency approaches 100%. Further work on improved fabrication techniques is under way.

4. Multistage interconnection network architecture

We have studied different optoelectronics MIN architectures and control algorithms[4] for constructing scalable MINs with the BCGH switch technological constraints. Two information routing algorithms are possible: centralized control, where an external control processor determines and configures all switch states, and distributed control with self-routing packet headers. In the latter case, the switch settings are calculated external to the network but the process of setting the switches is implemented using packet headers which propagate through the network and configure the "smart" opto-electronic spatial light modulator switch arrays during a dedicated header time interval. Once the switches in the MIN are set, the information may be both sent to and retrieved from the output nodes

through the same optical system at the speed of light, with a data modulation rate which is not limited by the network.

We have evaluated different interconnection network architectures (i.e., crossbar, N-stage planar, Batcher-Banyan, Benes, and Dilated Benes) in conjunction with their performance using BCGH technology in a passive all-optical network. For this study we computed the network attenuation losses and the network SNR vs the total number of switches using single switch insertion loss of -0.638 db and switch contrast ratio of 20 db. If we assume the maximum acceptable attenuation to be 30dB and the minimum SNR to be 11dB [5] then the maximum scalability (dotted lines) of the architectures can be estimated as shown in Figures 3 and 4.

We concluded from this study that the dilated Benes network[6], which is a rearrangeably non-blocking MIN, is well suited for large scale implementations of circuit-switched photonic interconnection networks using BCGH switching elements. Most importantly, the size of the network realistically possible using BCGH technology may be as large as 16,384 inputs with a 16 GHz data rate, well above the size and data modulation rate achievable with all-electronic networks.

5. Conclusions

In conclusion, we have introduced a method for constructing polarization-selective CGH using surface-relief etching of birefringent substrates. We tested this approach for a dual binary phase CGH fabricated in lithium niobate, yielding a diffraction efficiency was 6% and a 40:1 contrast ratio between polarizations. This element was used to experimentally evaluate a self-routing 1x2 polarization switch. Finally, we have examined technological implications of BCGH on optical MIN architectures.

This work was funded by Rome Laboratory under Grant F-30602-91-C-0094.

1. A. Ohba, Y. Kimura, S. Sugama, R. Katayama, and Y. Ono, Appl. Opt. 29, 5131-5135, 1990.
2. J. Ford, F. Xu, K. Urquhart, and Y. Fainman, "*Polarization selective computer generated holograms*," accepted by Optics Letters September 1992.
3. G. Swanson, M.I.T. Lincoln Laboratory Tech. Rep. 854, August 1989.
4. T. Cloonan, F. McCormick, and A. Lentine, OSA Tech. Dig., Topical Meeting on Photonic Switching, Salt Lake City, 1991.
5. N. Ailawadi, in Frontiers in Computing Systems Research Vol. 1, S. Tewksbury Ed., Plenum Press 1990.
6. K. Padmanaphan and A. Netravali, IEEE Trans. on Comm. C-30(12), December 1987.

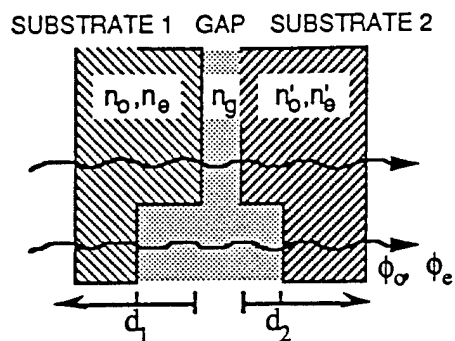


Figure 1. BCGH construction.

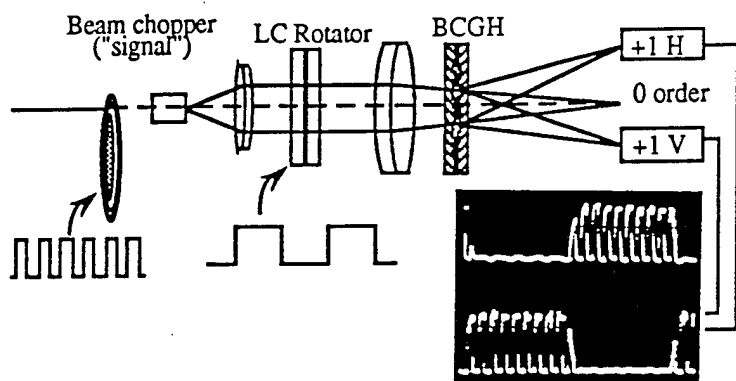


Figure 2. 1x2 polarization switch demonstration.

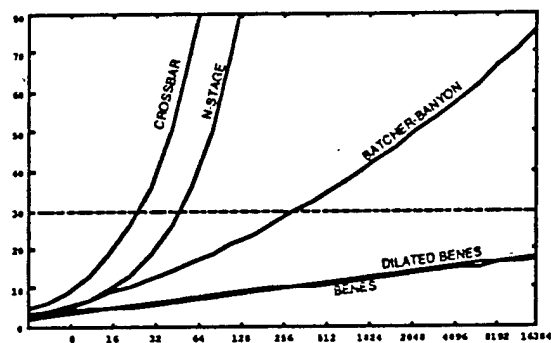


Figure 3. Network attenuation in db vs network size.

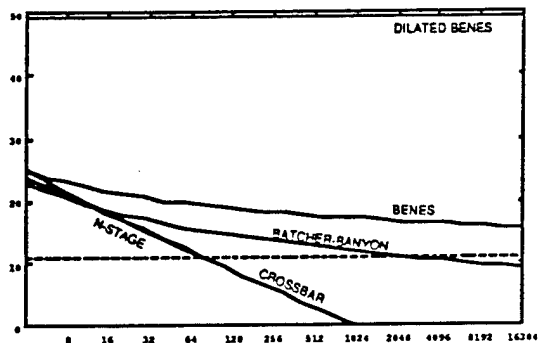


Figure 4. Network SNR in db vs size.

Appendix 3

Polarization selective computer generated holograms and applications

F. Xu, J. Ford and Y. Fainman

SPIE International Symposium on Optics, Imaging, and Instrumentation, Paper 1992-19, San Diego, CA July 1993.

Polarization selective computer generated holograms and applications

Fang Xu, Joseph E. Ford and Yeshayahu Fainman
Department of ECE, University of California San Diego, La Jolla, CA 92093-0407

ABSTRACT

Polarization sensitive diffractive optical elements are useful for free space optical interconnection networks and packaging. We demonstrate a multi-phase level polarization selective computer generated hologram with independent functionality for two orthogonal linear polarizations using lithium niobate substrate. The adjustments for design and fabrication of such an element are shown in this paper.

1. INTRODUCTION

Diffractive optics play an important role in constructing components for various optical systems. Diffractive optical elements are fabricated using microelectronics technology, which introduces such advantages as reliability, reproducibility, and cost-effectiveness. Diffractive optical elements have been used to implement various phase functions for such applications as aberration correction, optical filtering, free space optical interconnection, and opto-electronic packaging.¹ Conventional diffractive optical elements are made of isotropic materials and, therefore, are largely insensitive to light polarization. A computer generated hologram (CGH) that is sensitive to light polarization is desirable for numerous applications such as image processing, optical switching network, and opto-electronic packaging. The basic concept of a polarization selective CGH is shown in Fig. 1. Our main objective is to construct an optical element with independent functionality for two orthogonal linear polarizations that will collapse the functionality of a bulky and complicated optical system (see Fig. 1) into a single component. The following advantages are characteristic to our approach: (i) miniaturization, (ii) alignment with microfabrication accuracy.

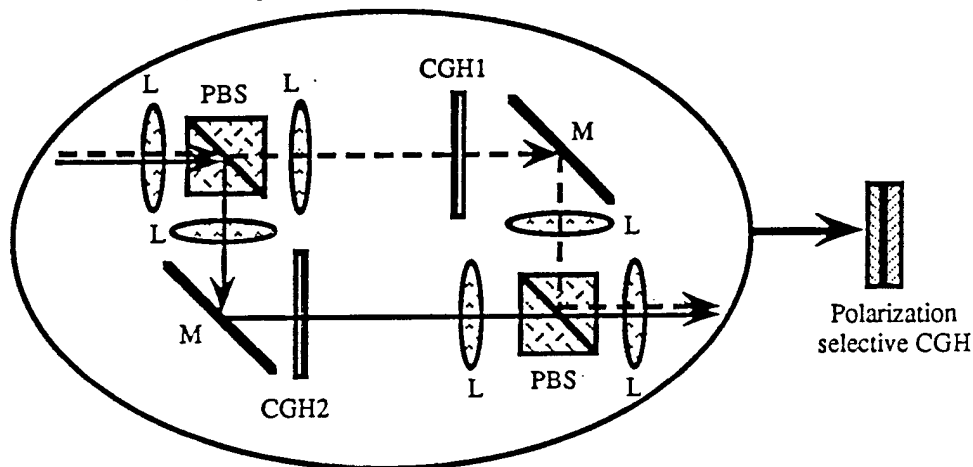


Fig. 1 Polarization selective CGH is a compact diffractive optical element with independent functionality for two orthogonal linear polarizations.

Polarization sensitive holograms have been optically recorded in organic dyes,² photorefractive crystals,³ and dichromatic gelatin.⁴ Diffraction grating polarizing beam splitters have been fabricated using high spatial frequency surface relief gratings.⁵ Our physical approach is related to that of Ohba et al⁶, where proton exchange in lithium niobate was used to create a birefringent grating, polarizing beam splitter. However, we use substrate birefringence to construct CGH with arbitrary diffractive functionality for the two orthogonal linear polarizations. Also, our fabrication technique is based on surface relief etching, allowing higher spatial resolution.

In the next section we introduce the principle of birefringent CGH (BCGH). In section 3 we describe the BCGH design methodology, while in section 4 we report the fabrication procedures. Experimental evaluation of the fabricated BCGH elements and their potential applications are presented in sections 5 and 6, respectively. Conclusions and future directions are given in section 7.

2. PRINCIPLE OF BCGH

A kinoform (phase only) CGH is a 2-D pixelated array of phase values. Normally, the absolute phase (substrate thickness) does not matter. We want to implement two arbitrary phase profiles -- one for each linear polarization -- on the same substrate. This can be accomplished by implementing two phase values at each hologram pixel (Φ_o and Φ_e) in terms of their phase difference ($\Phi_o - \Phi_e$) and their phase relative to some external reference such as an unetched pixel.

BCGH rely on diffraction of polarized optical waves from a surface relief grating fabricated in a birefringent substrate. A birefringent uniaxial crystal possesses refractive indices, n_o and n_e for ordinary and extraordinary polarized optical waves, respectively. A phase difference between these two orthogonal linear polarizations will result from propagation over a certain distance d inside the crystal along a specified propagation direction. Therefore, the phase difference of the desired impulse responses corresponding to the two orthogonally polarized waves can be implemented by controlling the distance, d . In diffractive optics this can be accomplished by controlling the etch depth of a plane-parallel birefringent substrate in a pixelated manner to get the desired phase differences for each pixel. However, the resultant relative absolute phase of the two impulse responses will be inaccurate. Therefore, we need to introduce an additional diffractive structure to set correct values of the relative phases, which can be accomplished by a surface relief profile etched into an isotropic substrate.

We use two surface relief holograms together and make them in contact.⁷ On both holograms, we have two independent etch depths d_1 and d_2 that allow to encode the two independent requirements on the phase difference and the absolute phase for the two impulse responses. In general, the BCGH can be made of two etched substrates of two different birefringent materials and a gap filled with a third media which might also be birefringent (i.e., liquid crystal but would normally be isotropic (i.e., air). Figure 2 shows the schematic diagram of a single pixel in such a hologram.

The optical path differences L_o and L_e corresponding to ordinary and extraordinary polarized light propagating through an etched pixel relative to an unetched pixel (see Fig. 2) is given by

$$\begin{aligned} (n_{1e} - n_{ge})d_1 + (n_{2e} - n_{ge})d_2 &= L_e \\ (n_{1o} - n_{go})d_1 + (n_{2o} - n_{go})d_2 &= L_o \end{aligned} \quad (1a)$$

where d_1 and d_2 are the etch depths in the two substrates, n_{1o} and n_{1e} are refractive indices in the first birefringent substrate for ordinary and extraordinary polarizations, respectively, n_{2o} and n_{2e} are refractive indices in the second birefringent substrate for ordinary and extraordinary polarizations, respectively, and n_{go} and n_{ge} are the refractive indices of the birefringent gap medium for ordinary and extraordinary polarizations, respectively.

Eq. (1a) can also be written in the form of phase differences,

$$\begin{aligned} (n_{1e} - n_{ge})\phi_1 + (n_{2e} - n_{ge})\phi_2 &= \Phi_e \\ (n_{1o} - n_{go})\phi_1 + (n_{2o} - n_{go})\phi_2 &= \Phi_o \end{aligned} \quad (1b)$$

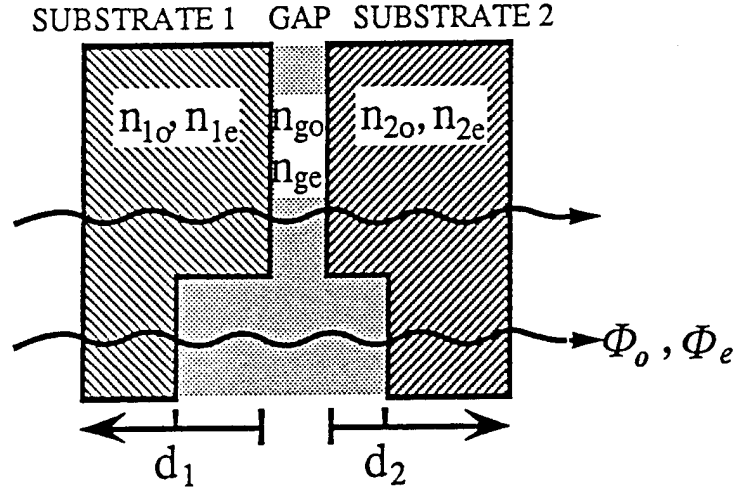


Fig. 2 The geometry of a single pixel in BCGH.⁷

where

$$\begin{aligned}\phi_1 &= k_0 d_1 = \frac{2\pi}{\lambda_0} d_1, & \phi_2 &= k_0 d_2 = \frac{2\pi}{\lambda_0} d_2 \\ \Phi_e &= k_0 L_e = \frac{2\pi}{\lambda_0} L_e, & \Phi_o &= k_0 L_o = \frac{2\pi}{\lambda_0} L_o\end{aligned}\quad (2)$$

and λ_0 is the wavelength of the optical wave in vacuum. Eq. 2 shows that in order to implement different and independent impulse responses for the two orthogonal linear polarizations, at least one of the substrates or the gap material must be birefringent. Figure 3 shows two examples of phasor diagrams for a BCGH constructed of (i) a birefringent and isotropic substrates with an isotropic gap medium (Fig. 3a) and (ii) two birefringent substrates with isotropic gap medium (Fig. 3b). In the first example (Fig. 3a), the etch in the first birefringent substrate introduces the desired phase difference for the two polarizations, while the second etch in the isotropic substrate sets the absolute phases for both polarizations. When the second substrate is also birefringent (Fig. 3b), then both substrates introduce phase difference between the two orthogonal polarizations as well as the absolute phases for the two orthogonal polarizations. In comparison, the BCGH constructed of two birefringent substrates will require smaller etch depths on both substrates.

In practice, we can use the same birefringent crystal with indexes n_o and n_e for both substrates of BCGH by rotating the optic axis of second substrate 90° with respect to the first one. For such arrangement the refractive indexes of the second substrate are given by

$$n_{2e} = n_{1o} = n_o \quad (3a)$$

$$n_{2o} = n_{1e} = n_e \quad (3b)$$

Also, let the gap medium be isotropic with refractive index n_g , then Eq. (1a) can be written as

$$\begin{aligned}(n_e - n_g)\phi_1 + (n_o - n_g)\phi_2 &= \Phi_e \\ (n_o - n_g)\phi_1 + (n_e - n_g)\phi_2 &= \Phi_o\end{aligned}\quad (4)$$

Unlike single substrate holograms, we have to consider free space propagation phenomena of light in the gap between the two surface relief diffractive structures. Usually the thickness of the

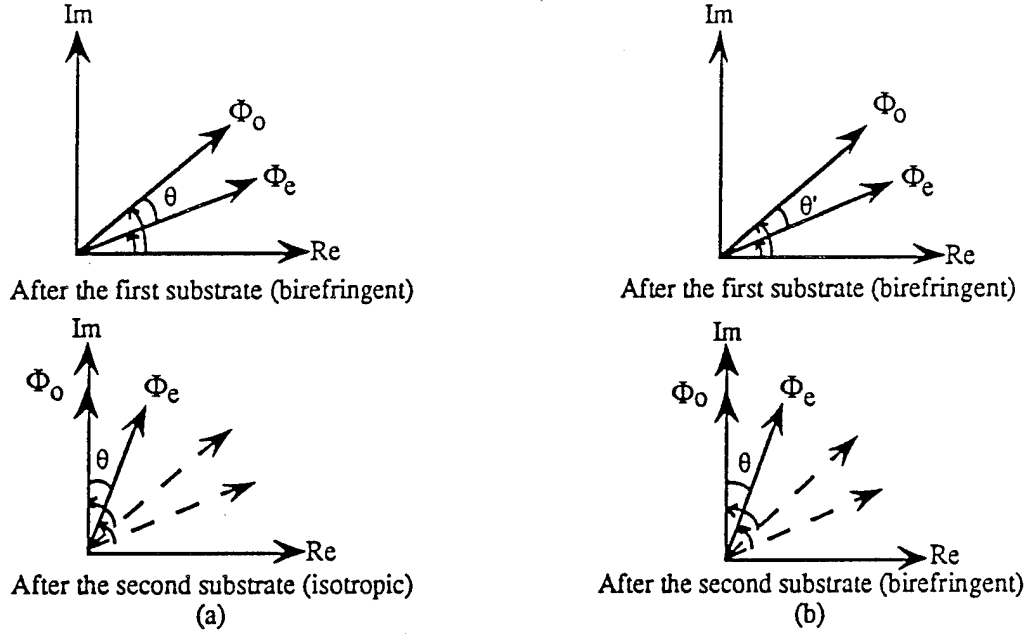


Fig. 3 Phasor diagram of a BCGH constructed of (a) a birefringent and isotropic substrates with isotropic gap medium and (b) two birefringent substrates with isotropic gap medium.

gap between the two substrates in unetched regions can be negligibly small (i.e., the gap between the two substrates is on the order of the substrate flatness which for optical surfaces is usually less than fraction of a wavelength). Therefore, since in diffractive optics single pixel size is on the order of few microns (in our experiments pixel size is $10\ \mu\text{m}$), we can ignore interference between adjacent pixels so that analysis using geometrical optics is justified. Furthermore, we consider antireflection coating of the diffractive structures so that the multiple reflections interference effects in the gap can be also ignored.

3. DESIGN OF BCGH

The design of BCGH elements is performed for commonly used diffractive optical elements fabrication procedures using electron beam (e-beam) lithography and etching a multi-phase-level surface relief microstructure. The design process of a conventional single element diffractive optical component with the desired phase function $\Phi(x, y)$ normally consists of (i) generating a function $\Phi'(x, y)$ which is modulo 2π version of $\Phi(x, y)$, (ii) choosing the number of phase quantization levels depending on the desired diffraction efficiency, and (iii) quantizing $\Phi'(x, y)$ to generate the data for masks to fabricate the quantized multi-level phase version of $\Phi_q(x, y)$. For example, $\log_2 N$ masks need to be designed and e-beam generated to fabricate an N-phase-level CGH.

However for BCGH, we need to implement two independent phase functions $\Phi_o(x, y)$ and $\Phi_e(x, y)$ for ordinary and extraordinary polarizations respectively. From equation (2) and (4) we obtain the required etch depths

$$d_1 = \frac{1}{k_0} \frac{(n_e - n_g)\Phi_e - (n_o - n_g)\Phi_o}{(n_e - n_g)^2 - (n_o - n_g)^2} \quad (5)$$

$$d_2 = \frac{1}{k_0} \frac{(n_e - n_g)\Phi_o - (n_o - n_g)\Phi_e}{(n_e - n_g)^2 - (n_o - n_g)^2}$$

For N phase quantization levels, Φ_o and Φ_e will be transferred into their discrete-valued versions Φ_{oq} and Φ_{eq} , respectively. Φ_{oq} and Φ_{eq} will take on one of the following values

$$0, \frac{2\pi}{N}, 2 \times \frac{2\pi}{N}, 3 \times \frac{2\pi}{N}, \dots, (N-1) \times \frac{2\pi}{N}$$

we can define two fundamental etch depth increments s_e and s_o ,

$$s_e = \frac{1}{N} \frac{\lambda(n_e - n_g)}{[(n_e - n_g)^2 - (n_o - n_g)^2]}$$

$$s_o = \frac{1}{N} \frac{\lambda(n_o - n_g)}{[(n_e - n_g)^2 - (n_o - n_g)^2]}$$
(6)

Eq. (5) then can be rewritten in quantized form in terms of the fundamental increments of Eq. (6) as

$$d_{1q} = \frac{N\Phi_{eq}}{2\pi} s_e - \frac{N\Phi_{oq}}{2\pi} s_o$$

$$d_{2q} = \frac{N\Phi_{oq}}{2\pi} s_e - \frac{N\Phi_{eq}}{2\pi} s_o$$
(7)

Since Φ_{oq} and Φ_{eq} are of N quantization levels, the corresponding quantized etch depths have in general a total of N×N different levels. Eq. (7) can also be written as

$$d_{1q} = as_e - bs_o$$

$$d_{2q} = bs_e - as_o$$
(8)

where

$$a = \frac{N\Phi_{eq}}{2\pi} \text{ and } b = \frac{N\Phi_{oq}}{2\pi}$$
(9)

a and b are integers 0, 1, 2, 3, ..., (N-1).

The quantized values d_{1q} and d_{2q} are depths etched into the flat surface and from practical fabrication considerations must be positive. To assure such a fabrication-imposed constraint we simply add a constant Ns_o to both sides of Eq (8) since in diffractive optics constant phase is of no concern. Eq. (8) can be then rewritten as

$$d'_{1q} = as_e + (N - b)s_o$$

$$d'_{2q} = bs_e + (N - a)s_o$$
(10)

where d'_{1q} and d'_{2q} are the positive etch depths for the two substrates, respectively. According to Eq.(10), d_{1q} and d_{2q} are both linear combinations of two independent variables s_o and s_e . We can design two sets of the corresponding e-beam masks for implementing the quantized multi-level etches d_{1q} and d_{2q} . Eq. (10) also shows that to fabricate an N phase level BCGH, we need $\log_2 N$ e-beam masks for implementing each term of the Eq. 7 (with Φ_{oq} and Φ_{eq}). Therefore, we need a total of

$4\log_2 N$ e-beam masks to implement d'_{1q} and d'_{2q} . This is four times as much as that for a single substrate diffractive optical element. However, by using the same birefringent material for the two substrates of BCGH we can fabricate both substrates simultaneously with a total number of $2\log_2 N$ etches.

4. BCGH FABRICATION

The birefringent material we use for fabrication of the BCGH element is a 1 mm thick Y-cut lithium niobate (LiNbO_3) crystal wafer of 3" diameter from Crystal Technology, Inc. We choose lithium niobate due to its optical quality, low cost, and relatively large birefringence ($n_o = 2.3325$ and $n_e = 2.2422$ at $\lambda = 514.5 \text{ nm}$). The crystal wafer is polished on both sides so that the wavefront distortion is better than $\lambda/4$ over a length of 1 cm (at optical wavelength of 633 nm).

To reduce the complexity and the time of the BCGH fabrication process, both substrates of the BCGH component are fabricated simultaneously on the same lithium niobate wafer. This is achieved by designing the e-beam masks for both substrates on the same e-beam plate where the corresponding two patterns are rotated by 90° with respect to each other. With this approach to BCGH fabrication the total number of required distinct etches is $2\log_2 N$.

For simultaneous fabrication of the two BCGH substrates, the lithium niobate wafer is cut into a $1" \times 2"$ rectangular shape. The lithium niobate substrate is first spin-coated by photoresist and the e-beam generated pattern for the first etch depth is transferred into the photoresist using standard microlithography procedures (soft bake, mask alignment, exposure, development of the photoresist, hard bake). The patterned lithium niobate substrate is then ion etched until the first desired etch depth is obtained. After the first ion etching is completed the photoresist is stripped off the substrate. Although ion milled photoresist is difficult to remove, we found that the nanostrip (96% sulfuric acid and 2% hydrogen peroxide, boiling point greater than 100°C) bathing for 10 - 20 minutes at 90°C removes the photoresist effectively. Identical fabrication procedures are repeated for the remaining etch depths, resulting in the desired surface relief microstructure on the surface of the lithium niobate substrate.

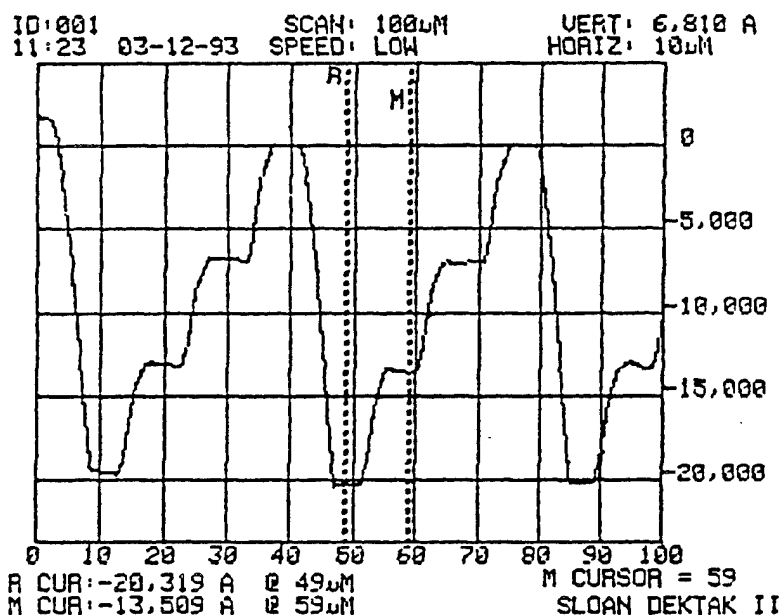


Fig. 4 Surface relief profile measured by Dektak

The etch depth of each fabricated surface relief was measured by a Dektak IIA surface profiler. Fig. 4 shows an example of a single scan of such a profile. We selected at random 10 data

points from the measured results and calculated the average value, \bar{d} . We defined etch uniformity, U as the ratio

$$U = \frac{\text{Max}(|d_i - \bar{d}|)}{\bar{d}} \quad (11)$$

where $\text{Max}()$ is defining the maximum value operation and d_i is the measured etch depth at $i=1, 2, \dots, 10$ sampled points. For the BCGH elements that have been fabricated we found that the accuracy of the measured etch depth was within 3% of its designed value with etch uniformity better than 5%

When the etching process was completed, we have cut the lithium niobate 1"x2" etched wafer into the two 1"x1" substrates, which must be assembled face-to-face to complete the fabrication of the BCGH. The two separate substrates with the surface relief microstructures must be aligned with high accuracy. We have considered and used two methods: (i) assembly with a mask aligner and (ii) assembly using in situ optical alignment/testing. For assembly using the mask aligner we introduced alignment marks (e.g., cross and diamond pair) on the e-beam mask. These marks were ion etched into the substrates during the fabrication and used later to align the two substrates in the mask aligner. The principle of the in situ alignment is based on illuminating the patterns on the two lithium niobate substrates in contact with a collimated laser beam and real time observation of the resultant diffracted field using a CCD camera. Using high resolution translation and rotation stages, we maximize the desired performance of our BCGH element and then apply the UV cured epoxy, cured with hand-held UV light source. As an alternative, we also designed additional alignment features such as gratings, incorporated in the e-beam mask. These features generate Talbot effect and Moiré patterns, which are analyzed and used to achieve accurate alignment.

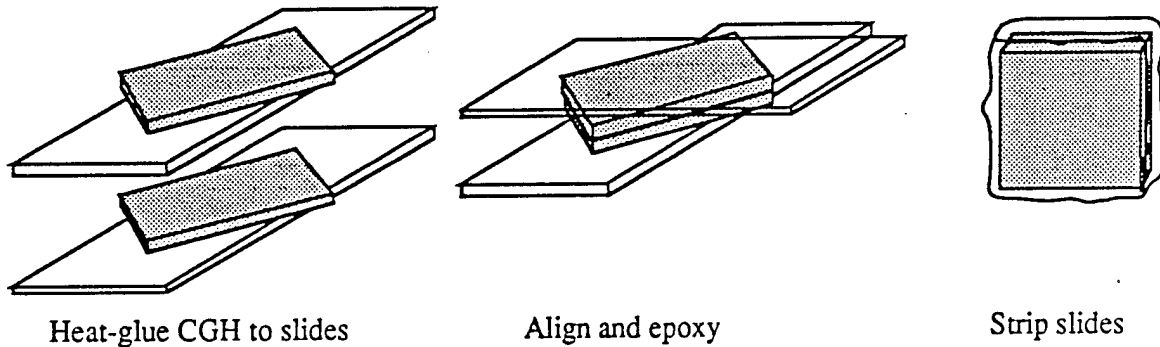


Fig. 5 Schematic diagram for BCGH assembly

The procedure for both assembly methods is shown schematically in Fig. 5. The assembly process includes temporary bounding of the BCGH substrates to larger glass substrates that can be held in the mask aligner and the in situ assembly setup. This bounding is obtained using a heat release glue. After the bounded BCGH substrates are aligned in the mask aligner or the in situ assembly setup, the two lithium niobate plates are bounded together using UV cured epoxy. Finally, the assembled BCGH is heat released from the glass substrates. The residue of the heat release glue is removed using acetone.

To reduce the reflection losses, we have also coated the BCGH substrate before assembly with an anti-reflection (AR) coating. We evaporated a silicon dioxide (SiO_2) thin film (of thickness $\lambda/4$ to operate at $\lambda = 514.5$ nm) using an ion-plating evaporation system. The reflectance of AR coated single substrate of lithium niobate was measured to be $0.4 \pm 0.1\%$. Compared to uncoated BCGH, the reflection loss is reduced from 49% to less than 1%. Fig. 6 shows the transmission of lithium niobate substrate with both sides AR coating as a function of wavelength.

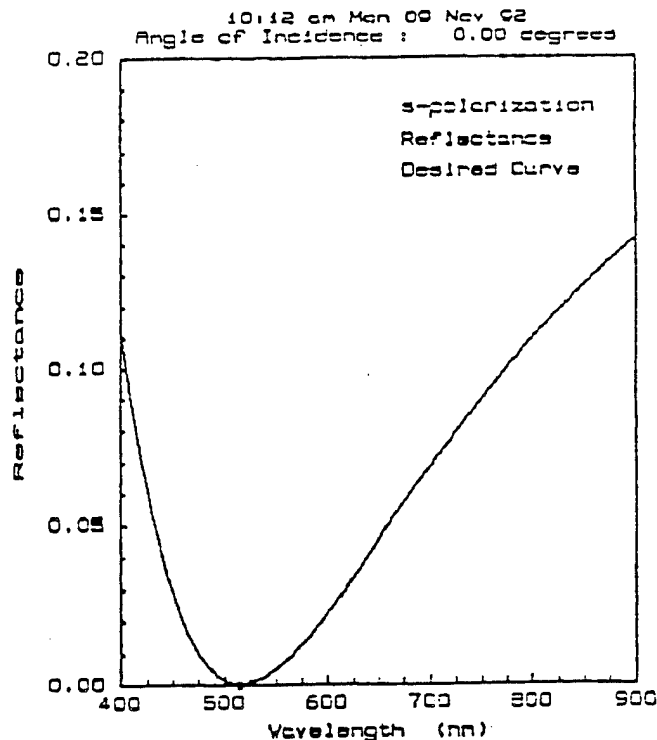


Fig. 6 Reflectance of AR coated LiNbO₃ substrate

5. EXPERIMENTAL EVALUATION OF BCGH

A collimated laser beam is used for reconstruction of the fabricated BCGH elements. The diffraction efficiencies (ratio of the diffracted power into the desired order to that of the total transmitted power) for *binary* phase BCGH elements were measured varying from 6% to 25%. The maximum contrast ratio (i.e., ratio between the powers of the diffracted beams at ordinary and extraordinary polarizations) was measured 40:1.⁷

Recently, we have designed and fabricated a four-level-phase BCGH element. This element was designed for application in a multistage interconnection network consisting of 16 nodes. This BCGH is a four-level phase element consisting of 4x4 array of blazed gratings. The grating periods are 40 μm while the smallest feature size in the hologram is 10 μm which is the same that in our binary phase holograms. The measured diffraction efficiency was 26.3%. The maximum contrasted ratio was 130:1.

6. APPLICATIONS

We have constructed a number of BCGH elements that implement two independent impulse responses for the two orthogonal linear polarizations. These elements were designed for three different free-space optics applications: image processing, interconnection networks and packaging optoelectronic devices and systems.

6.1 Image processing

We designed and fabricated a birefringent lens with dual focal length for the two orthogonal polarizations. One of the focal lengths (e.g., for horizontally polarized light) is twice as long as the other (e.g., for the vertically polarized light). This BCGH element depending on polarization can perform imaging and Fourier transformation of a two-dimensional object to a single output plane without any mechanical motion (See Fig. 7(a)). Fig. 7(b) shows the photographs of the image and the

Fourier transform of an object (e.g., characters "UCSD") performed by our BCGH dual focal length lens. The two results are obtained by simply changing the polarization of the light illuminating the input transparency.

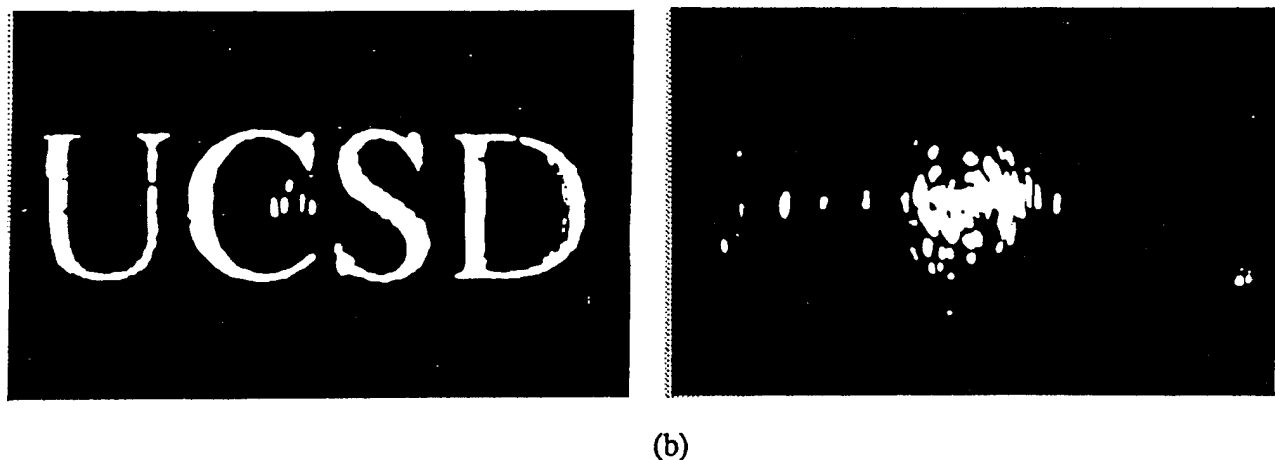
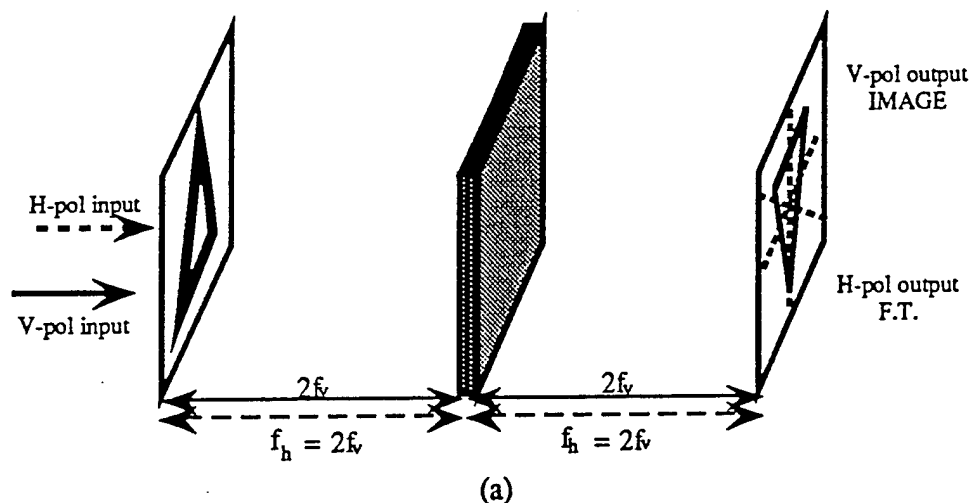


Fig. 7 Imaging and Fourier transforming at same plane without any moving parts

6.2 A 2×2 optical switch for interconnection networks

A 2×2 switch can be built from two 1×2 switches. Since a dual BCGH beam splitter (including focusing function) can be seen as a 1×2 switch, we can construct a 2×2 switch as shown schematically in Fig. 8. The polarization rotator sandwiched between the two BCGH elements controls the function of the 2×2 switch, i.e., either cross-over or straight-through. The first hologram combines and focuses the two inputs into the modulator, which either exchanges their polarizations or not. The second hologram separates and directs the outputs to their destinations. Since optical path is reversible, this element will have same functionality for beams propagating in reverse.

The schematic diagram of our optical setup for demonstration of the 2×2 switch is shown in Fig. 8. We use two beam choppers to modulate the two orthogonally polarized input beam at different frequencies (i.e., to simulate two information channels). The first BCGH element is a dual beam splitter which deflects the horizontally and vertically polarized light into two different directions. The two modulated beams propagating in different directions at the input are combined by the first BCGH element and both propagate in the same direction through liquid crystal (LC) polarization rotator. The

second BCGH element implements a dual beam splitter deflecting the two beams into two different directions. The output beams are detected by two photodetectors. If the LC is in the off-state the two beams propagate straight through. When the LC is turned on, the two beams cross-over at the output. In our experiment we have applied a square wave voltage to the LC causing periodic switching of the light beams between the two output photodetectors. The oscilloscope trace photographs of our experimental results are shown in Fig. 8(b) demonstrating switching of information between the two channels at the output. The signal to noise ratio (SNR) for a single 1×2 switch was measured as 25:1.

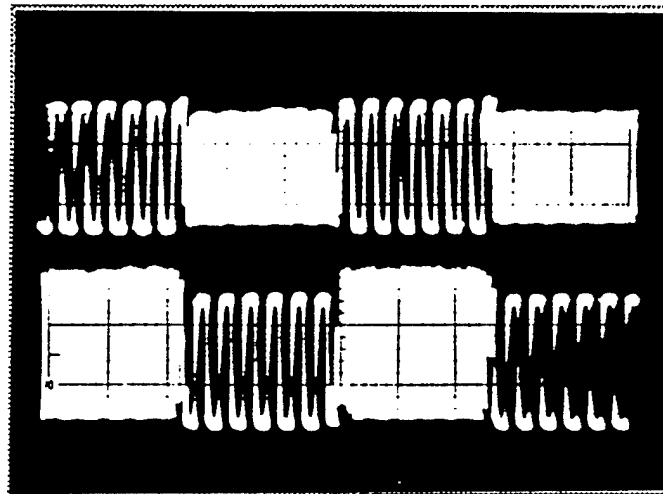
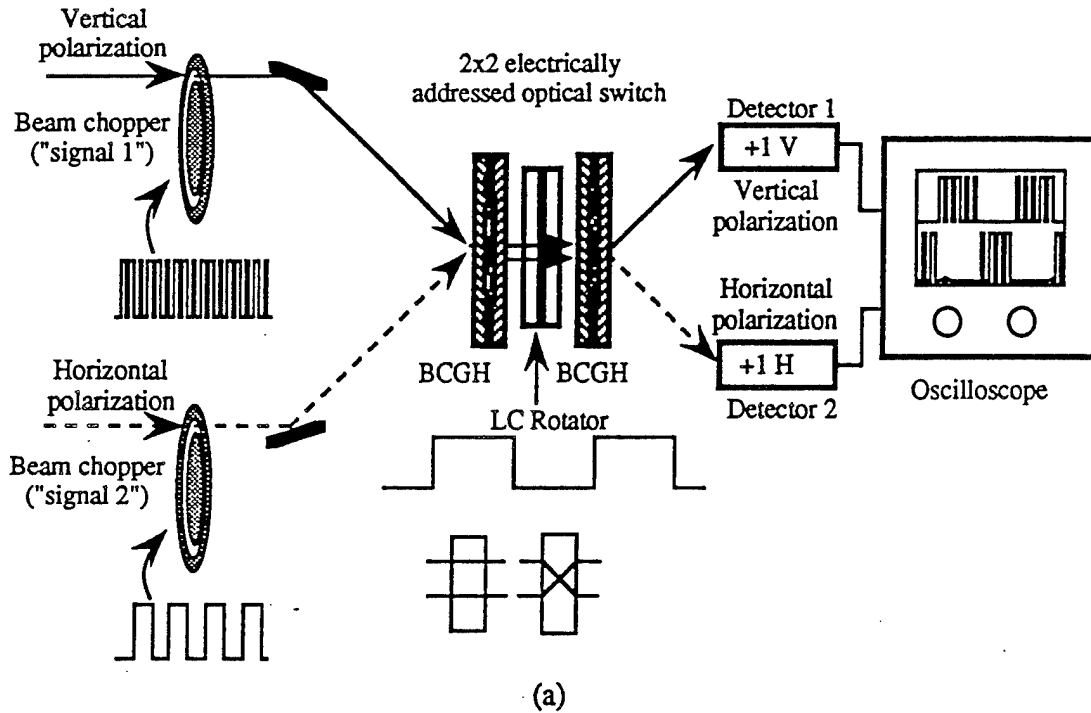


Fig. 8 Schematic diagram of the setup of a 2×2 switch demonstration and oscilloscope trace

The polarization rotator limits the switching speed of the 2×2 switch. In our demonstration, a liquid crystal polarization rotator was operated at a switching rate about 1 KHz. If we use a PLZT or multiple quantum well (MQW)-based polarization rotator, switching as fast as 10MHz to 100MHz can be achieved^{9,10} Such polarization sensitive switches are promising for construction of large size ultra-

high speed interconnection networks applications because they do not require signal regeneration. Once the polarization switch is set the data transmission rate is determined only by the speed characteristics of transmitter and receiver.

6.3 Opto-electronic packaging

An additional interesting and important application of BCGH is packaging opto-electronic devices and systems. For example, BCGH can implement arbitrary dual functionality, which could be useful for addressing smart pixel arrays that utilize both modulators and laser sources. In our example shown in Fig. 9, the BCGH element simultaneously performs routing of optical information to the photodetectors and from the light sources in each pixel of the 2-D array.

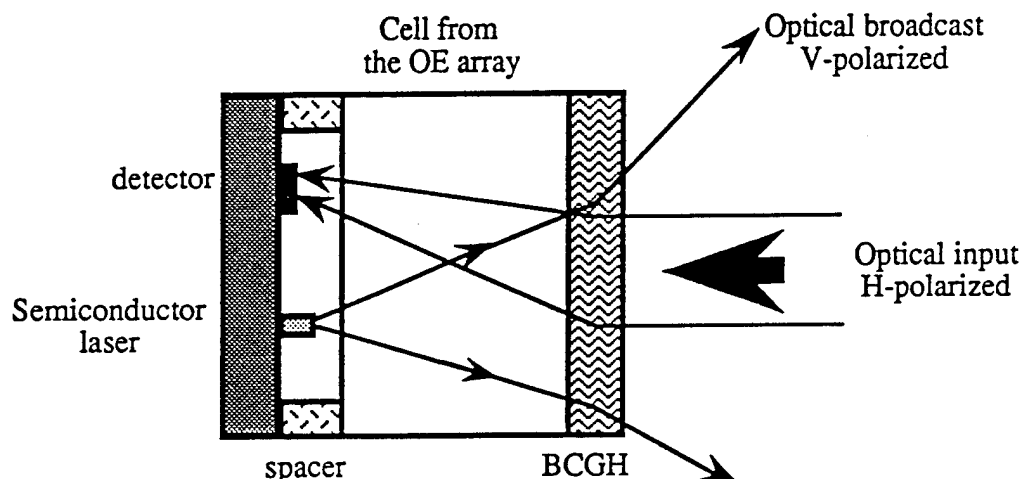


Fig. 9 Packaging opto-electronic device using BCGH: single pixel from a 2D smart pixel array

7 CONCLUSIONS

Polarization selective computer generated holograms have been designed, fabricated and evaluated. Design methodology for multilevel phase BCGH elements was developed. Fabrication techniques using microelectronics technology have been adjusted for BCGH fabrication. Special diffractive features for accurate BCGH assembly have been developed and used for BCGH assembly with mask aligner and in situ alignment/testing/assembly techniques. The BCGH element has been AR coated to increase the light transmission efficiency. The fabricated BCGH elements have been evaluated experimentally demonstrating good performances.

We have constructed and demonstrated experimentally BCGH elements that are useful for such application as image processing, optical switching and packaging optoelectronic devices and systems. In particular, we have demonstrated experimentally a dual focal length lens for image processing applications, and constructed and evaluated a 2x2 optical switch for optical interconnection network applications.

In the future we plan to continue the research on BCGH elements by exploring fabrication of BCGH in birefringent polymers and other birefringent substrates that possess low refractive index and high birefringence. We are also exploring design and fabrication of single substrate BCGH using form birefringence. Finally, we are considering new applications of BCGH components.

7. ACKNOWLEDGMENTS

The authors want to thank Brian Sullivan and Allan Waldorf of National Research Council,

Canada for their optical coatings, and Hughes Aircraft Company for their loan of a liquid crystal polarization rotator. We also thank Dr. Sadik Esener, Dr. Sing Lee, Walter Däshner, Dr. Jinghua Wang, Dr. Jian Ma, Dr. Volkan Ozguz, Brian Catanzaro, Susan Hunter, and Dr. Subramania Krishnakumar for their valuable contributions. This work was funded by Rome Laboratory under Grant F-30602-91-C-0094.

8. REFERENCES

- 1 S.H. Lee, Ed, SPIE Milestone Series, Vol MS 33, 1992.
- 2 T. Todorov, L. Nikolova, K. Stoyanova, and N. Tomova, Appl. Opt. 24, 785-788, 1985.
- 3 Q. W. Song, M. C. Lee, P. J. Talbot, and E. Tam, Opt. Lett. 16, 1228-1230, 1991.
- 4 R. Kostuk, M. Kato, and Y. T. Huang, Appl. Opt. 29, 3848-3854, 1990.
- 5 A. Ohba, Y. Kimura, S. Sugama, R. Katayama, and Y. Ono, Appl. Opt. 29, 5131-5135, 1990.
- 6 A. Ohba, Y. Kimura, S. Sugama, Y. Urino, and Y. Ono, Jpn. J. Appl. Phys. 28, Suppl. 28-3, 359-361, 1989.
- 7 J. Ford, F. Xu, K. Urqhart and Y. Fainman, Opt. Lett. Vol 18, No. 6, 456 - 458, 1993.
- 8 Lithium niobate Optical Crystals data sheet, Crystal Technology, Inc.
- 9 C.J. Kirkby, Appl. Opt, Vol. 15, No. 4, 828-830, 1976.
- 10 M. Wraback, *et. al*, Quantum Optoelectronics Technical Digest, 1993, 98-99.

Appendix 4

Architectural considerations for MINs based on BCGH technology

In preparation for publication

Architectural considerations for MINs based on BCGH technology

Ashok Krishnamoorthy, Joe Ford, Sadik Esener, Shaya Fainman

6/20/92

Abstract: We describe an optoelectronic circuit-switched multistage interconnection network which can be used with birefringent computer generated hologram (BCGH) technology to provide rearrangeably non-blocking multistage interconnection networks (MIN) with either centralized or distributed control. In both cases, data is transmitted with time-of-flight delay without requiring electrical to optical conversions. This allows data transfer rates into the GHz regime and beyond. We compare several architectures and show the feasibility of implementing rearrangeably non-blocking $\Theta(2\log N)$ stage (Benes) networks with BCGH technology.

Table of contents

1. Introduction and objectives	52
(a) Existing technology	
(b) Goals for photonic MINs	
2. BCGH Technology for MINs	53
(a) BCGH technology	
(b) Use of BCGH as an optical switch for MINs	
(c) Circuit switched algorithms and control	
3. Circuit switching: operations and control	55
(a) Definitions	
(b) Control algorithms and architectures	
4. Interconnection network architectures	57
5. Architecture comparison / feasibility analysis	61
6. Discussion and conclusions	63
7. References	64
Table 1: Architecture comparison	65

1. Introduction and objectives

1(a) Existing technologies

The objective of the project was to design a high data rate interconnection network that would far exceed the capabilities of state-of-the-art electronic networks. Existing designs for VLSI based interconnection networks can be separated into two main categories, MINs and crossbars. Both have been implemented only with VLSI to date.

(i) VLSI-based Crossbars

Crossbars were the first type of VLSI interconnection networks. They use nearest neighbor (mesh) interconnections in a $N \times N$ array of switches. 64×64 prototype chips with bandwidths in excess of 200 Mbits/channel have been demonstrated. The number of switches a signal passes through ranges from 1 to $2N-1$, introducing signal skew. Skew can only be corrected by slowing the network speed to the longest delay. Larger networks can be assembled from smaller crossbar chips with, however, a reduced bandwidth/channel.

(ii) VLSI-based MINs

Multistage interconnection networks were introduced to reduce the chip area dedicated to switches. They typically require $O(N \log_2 N)$ switches instead of N^2 for the crossbar. These networks have data rates in the 100 Mbit/sec range. Prototype VLSI chips with 32 inputs and 32 outputs (32×32) self-routing networks have been built (Ref [1]). These networks can take up to several hundred inputs by use of several chips, again with an associated loss of bandwidth per channel. Such networks do not scale well, as the bandwidth/channel drops rapidly beyond network sizes of 256 (Ref [2]).

The locally-interconnected topology of a crossbar places more of the burden on processing area, while the globally-interconnected MIN puts the emphasis on interconnection wires. As the network size and longest line-length increase, the costs of communication in all-electronic processing tends to dominate. This makes crossbar networks the most effective approach for large-scale applications. However, if the communication costs could be reduced then the primary advantage of MINs, the lower switch count, would make them more attractive than crossbars. Optical interconnection offers the potential for a significant reduction in communication costs, especially at the long distances characteristic of large interconnection networks.

1(b) Goals for photonic interconnection networks

Based on the above considerations, to be competitive with VLSI we need to be in one of the following categories:

- (1) Network size $N > 256$ I/O channels with bandwidth/channel > 100 Mbits/sec
- (2) Network size $N > 64$ I/O channels with bandwidth/channel > 500 Mbits/sec
- (3) Any size network with data rates in excess of 1 Gbit/sec

We must also consider other technologies such as GaAs which could potentially provide Gbit/sec links. Therefore we would like to implement alternative (3) with network sizes $N \geq 256$:

GOAL: Interconnection network with $N \geq 256$ channels and $BW / \text{channel} \geq 1 \text{ Gbit/sec}$

2. BCGH Technology for MINs

2(a) BCGH Technology

For a description of BCGH technology, see the RADC interconnection project proposal (Ref [3]). The idea, in brief, is a computer generated holographic optical element fabricated in a birefringent media (hence BCGH) which produces an independent impulse response for each of the two orthogonal linear polarizations of the input light.

2(b) Use of BCGH as an optical switch for MINs

Two types of switches can be used for MINs (Ref [1]), 1x2 and a 2x2 switches. Both are binary state devices

(i) 1x2 Switch:



Figure 1: 1x2 Switch

A switching MIN network can be made with $\vartheta(\log_2 N)$ stages of N switches per stage and $2N$ links between stages (see Appendix). This type of network is generally classified as a graph (Ref [4]) model MIN. Switching is achieved by the choice of output link each input takes.

(ii) 2x2 Switch:



Figure 2: 2x2 Switch

A switching MIN network can be made with $\vartheta(\log_2 N)$ stages of these switches with $N/2$ switches per stage and N links between stages (see Appendix). This type of network is generally classified as a circuit model MIN. Switching is achieved by choice of 2x2 switch states.

It is possible to build a 2x2 switch using 1x2 switches (in fact, that is the way it is usually done. Refs [1,2,5]):

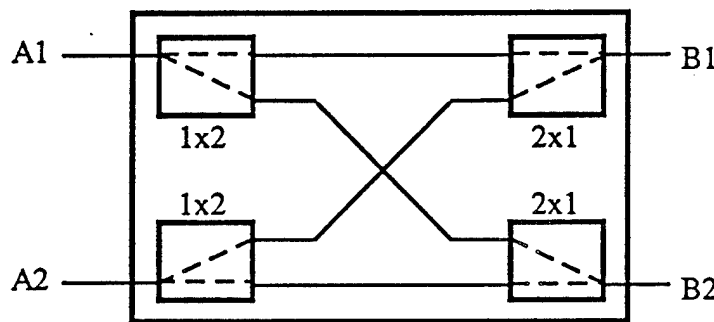
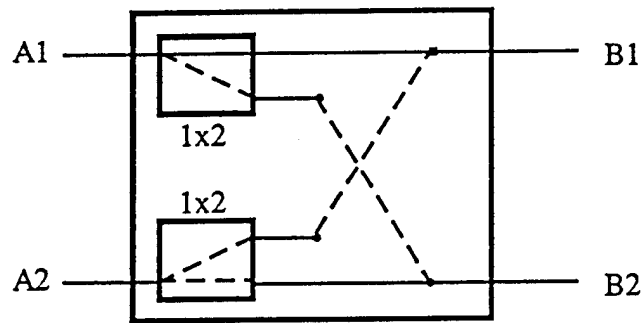
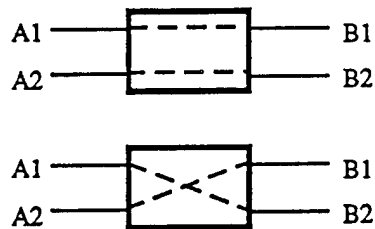


Figure 3: 2x2 switch constructed using 1x2 switches. (Control and clock not shown)

The basic idea of the 2x2 switch using 1x2 switches can also work for passive switches (i.e. BCGH) as long as certain configurations can be avoided. Because the switch is binary, both inputs can share a single actual switching element (i.e., polarization rotator) is necessary. However, two BCGH optical elements are necessary; one to guide both inputs through the rotator and another to direct the output. The optical switch design will be discussed in more detail in section 5.



Allowed configurations



Disallowed configurations

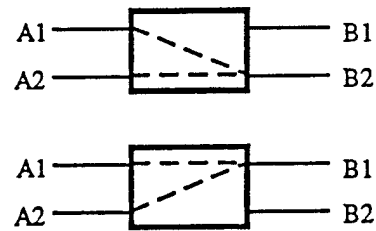


Figure 4: 2x2 switch using passive 1x2 switches.

Conclusion: BCGH technology allows us to build a switching network with 2x2 switches in the circuit model with N links per stage and two BCGH components per stage OR a graph model switching network with $2N$ links per stage and one BCGH component per stage.

Both networks operate in passive mode. That is, there is no electronic detection and optical signal regeneration. The disallowed configurations will be avoided by a suitable control algorithm, as will be discussed next.

3. Circuit switching: Operation and control

3(a) Definitions

Circuit switching is the dominant network paradigm for both voice and data communications in modern telecommunications, and data communications in computer systems.

Definition: Circuit switching implies that there is a dedicated communication path between the communicating nodes. The path is a sequence of physical links between network nodes. Communication involves three phases:

- (i) Circuit establishment: end-to-end circuits made before transmission begins
- (ii) Data transmission
- (iii) Circuit disconnect

Circuit switching can be achieved through space division switching (SDS) or time division switching (STS). Note that the networks here are of the space division switching type to be used for high-performance telecommunications systems or for parallel computers, with the added possibility that the inputs to the network may be time-division multiplexed from an optical fiber bundle. This is important in view of the high data rate which the network will be capable of supporting.

⇒ GHz bandwidth / channel possible using high speed lasers for modulation in BCGH networks.

3(b) Control algorithms and architecture

Four distinct types of circuit switching control algorithms can be defined (Ref [6]).

(i). Centralized control with global switching

Here, the switches in each layer of the network are linked, and can only switch as a unit. The major advantage of this approach is that the switches are simple bulk modulators, rather than pixellated arrays, making the network very easy to construct. However, only a single arbitrary interconnection of one input to one output can be made at one time. Either the interconnections must be multiplexed in time N , or a limited subset of interconnections used. This method is clearly of little or no interest for most applications. It is useful only as a preliminary laboratory demonstration step in the development of efficient switches.

(ii) Centralized control with direct injection

In this scheme the routing algorithm is calculated at a central controller which has direct and independent connections to every switching node (possible through an intermediate memory module which accesses the elements sequentially or in a semi-parallel fashion). This is a way of implementing pure circuit switching, exactly analogous to that done in electronic telecommunications networks. This method is not very scaleable; pin-out problems from the central controller seriously impedes the growth of the network. The time required to load the switch states grows linearly (at least) with N . Parallel optical loading could in principle be used where an external spatial light modulator (SLM) images the switch state information onto the switch array. This merely moves the switch setup problem to the SLM, with no improvement in performance. This approach is therefore only interesting for BCGH MINs as an intermediate demonstration step.

(iii) Centralized control with packet headers

This is an interesting approach for BCGH MINs in that it offers capabilities and characteristics different from any existing MIN. The routing algorithm is performed at a centralized controller, but the process of setting the switches is implemented using packet headers which propagate through the network. This can be achieved using only a few (<50) transistors per switch and can be achieved using BCGH coupled with smart SLM technology. The routing information must still be distributed to the data source array, but not to the arrays at each layer of the network. The rearrangeably non-blocking MINs discussed in the next section will be amenable to such an implementation. The difference between the existing packet switched networks and the BCGH MIN is that we can perform "virtual" circuit switching by specifying a dedicated header time interval for the packet headers with control information to propagate through the network and set up the required data paths. This will then allow the passive transmission (no detection and rebroadcast costs) at high data rates. The disadvantages of this approach are that it requires synchronous network operation and a more complex ('smart') SLM technology. One main advantage is a reduced controller pin-out (a factor of at least $\log_2 N$ fewer than direct injection). The secondary advantage is that this is an evolutionary step towards the self-routing network as described next.

(iv) Distributed control with self-routing packet headers

This type of routing algorithm is very promising for BCGH MINs with smart SLMs. This algorithm is typically associated with packet switching, where a short burst of information travels through the network by being received, briefly stored, and rebroadcast at each node (see Ref 5). A smart pixel implementation will require about 100 transistors per 1×2 switch ([5]). This approach uses the same smart SLM hardware and interconnection topology as approach (iii). The difference is in the control. Moving the routing to a centralized controller presupposes global interconnection within the controller, albeit at a substantially reduced speed. Here no centralized controller is necessary. This can be a major improvement in cost and scalability. However, the issues of contention and blocking must be addressed either in the hardware (network configuration, size, and switch capability) or software (control and routing algorithms).

The BCGH MIN system for approaches (iii) and (iv) will operate in a synchronous mode. In front of each smart SLM will be a bulk electro-optical modulator whose purpose will be to shift the data stream to an array of detectors controlling the switch states. The modulator is momentarily activated during the point of the header time interval when the address information corresponding to that layer of the network is sent. This way only the part of the packet header needed for that switch will be detected and used. After the header time interval has elapsed the switches will be set according to the packet

headers and high-speed passive data transmission can continue. Note that an alternative approach where a fraction of the signal is permanently deflected to the switch detector is inferior for two reasons; (i) more complex electronics at each switch to select the proper data bit, and (ii) unacceptably high power losses for a passive network.

Conclusion: Competitive photonic circuit switching can be achieved using BCGH technology together with smart SLM technology to implement either centralized control OR distributed control with packet headers. The former is well suited to the non-blocking or rearrangeably non-blocking networks (e.g. crossbar, Benes, Dilated Benes, and N-stage) discussed in the following section. The latter approach achieves "virtual-circuit" packet switching (a hybrid between circuit and packet switching) and is well suited to all the networks discussed next including the Batcher Banyan network.

4. Interconnection network architectures

In the following we describe some architectures that are suitable for implementation with the 2x2 BCGH switches.

1. Crossbar

This is a well known architecture with N^2 switches and a worst case path length of $2N-1$. Note that the number of stages and therefore the signal skew depends on the particular interconnection. The connection is a nearest neighbor "mesh" pattern which can be implemented optically as shown in Figure 5.

2. N-Stage planar

The N-stage planar (Figure 6) is a rearrangeably non-blocking architecture requiring N stages with $N/2$ switching elements per stage (see Ref [7]). It was an evolutionary development from the crossbar (think of Figure 5 stretched until the diagonal lines are horizontal), also using nearest-neighbor interconnections. The total number of switches is $N(N+1)/2$ and the maximum path length is N.

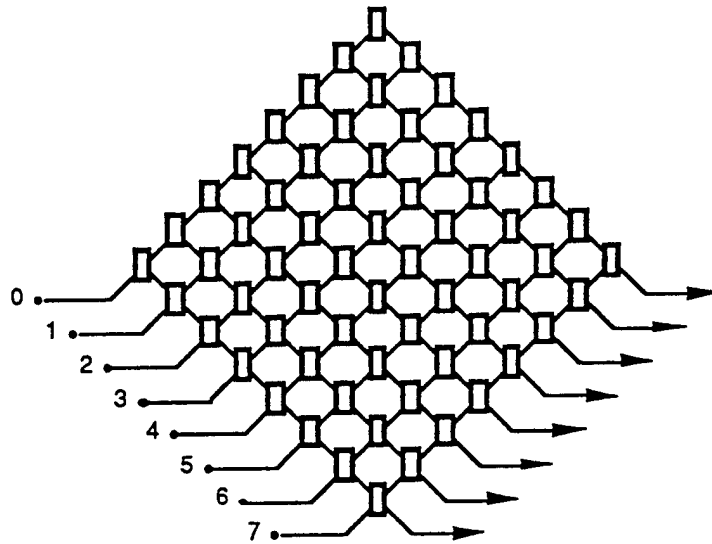


Figure 5: Crossbar network using N^2 switches and a mesh interconnection topology.

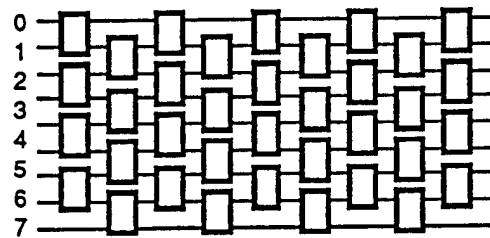


Figure 6: N-stage Planar network using $N(N+1)/2$ switches.

3. Benes network

The Benes network (Ref [8]) consists basically of two $\log_2 N$ networks placed end to end (see Figure 7). The network has $2\log_2 N - 1$ stages, which is the theoretical minimum number of stages required for rearrangeably non-blocking operation. The type of interconnection pattern used can be any binary permutation network, including the butterfly shown in Figure x2 as well as the crossover, shuffle exchange, etc. This is a globally interconnected topology, unlike the crossbar and N-stage networks.

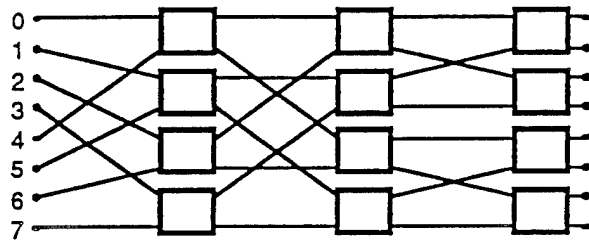


Figure 7: 8x8 Benes network using butterfly interconnection pattern

4. Dilated Benes network

This architecture was originally invented for waveguide couplers, which tend to have significant crosstalk. This is a Benes network which has been doubled in width while maintaining the initial number of inputs and outputs (Ref [9]). The first and last layers are 1x2 and 2x1 switches, respectively (Figure 8). The network has the unique advantage that no switching element carries more than one active signal. The full capability of the optical switches, simultaneously carrying signals along two intersecting paths, is not used. In exchange, noise can only get into the signal line by passing through two nominally 'off' switches. If second order crosstalk is negligible (usually true), then the network has a theoretically infinite signal to noise ratio (SNR). Dilated Benes networks have $2\log_2 N$ stages and N switches per stage.

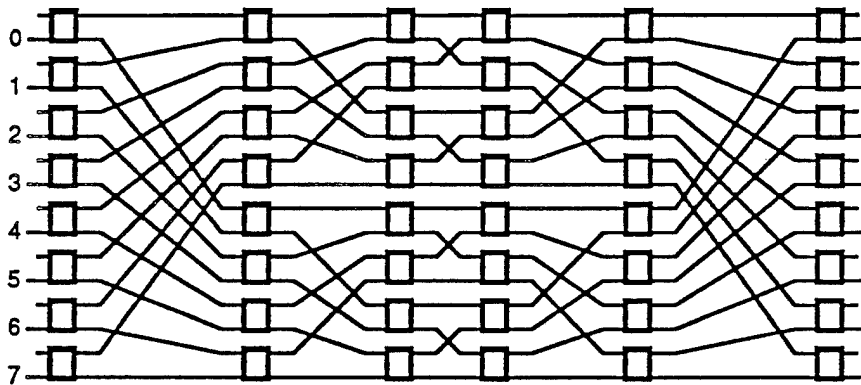


Figure 8: 8x8 Dilated Benes network using butterfly interconnection pattern

5. Batcher-Banyon network

The Batcher-Banyon network (Figure 9) is a self-routing network consisting of a sorting network followed by a routing network. This is nominally a packet-switched architecture but can be used in a

"virtual" circuit architecture as described in Section 4. The total number of stages is equal to $\frac{1}{2} \log_2 N (\log_2 N + 1) + \log_2 N$. This network is topologically equivalent to a large class of binary networks including the shuffle-exchange network.

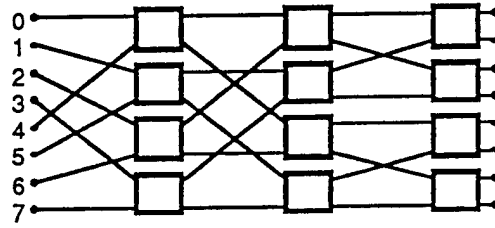


Figure 9: Batcher-Banyon network.

5. Architecture comparison / feasibility analysis

5(a) BCGH components

(i) Insertion loss calculation for a single BCGH switch node

A single BCGH switching element is shown in Figure 10. The function of the optical switch shown is identical to the 2x2 switch shown in Figure 2. The disallowed states shown in Figure 4 are avoided by fixing the input polarizations so that one polarization always goes 'up' (to a designated half of the network) and the other always goes 'down'. The sources of optical loss are reflections from the dielectric surfaces and the diffraction efficiency of the holograms. A silicon processing chip is necessary for smart SLM operation. Depending on the particular device technology, this will introduce additional surfaces (for example, a common sapphire substrate holding both the silicon and modulator materials) or not (if a silicon chip with openings etched into it acts as the substrate). However, the calculations presented here are representative of the realistic switch performance obtainable.

Surface reflections losses come from the BCGH substrate (R_g) and the modulator substrate (R_m). Clipping loss C occurs when the beams are focused through an aperture at the modulator. The finally source of loss is the diffraction efficiency of the holograms η . The total switch efficiency is then $\eta_{\text{switch}} = \eta^2 R_g^8 R_m^2 C$.

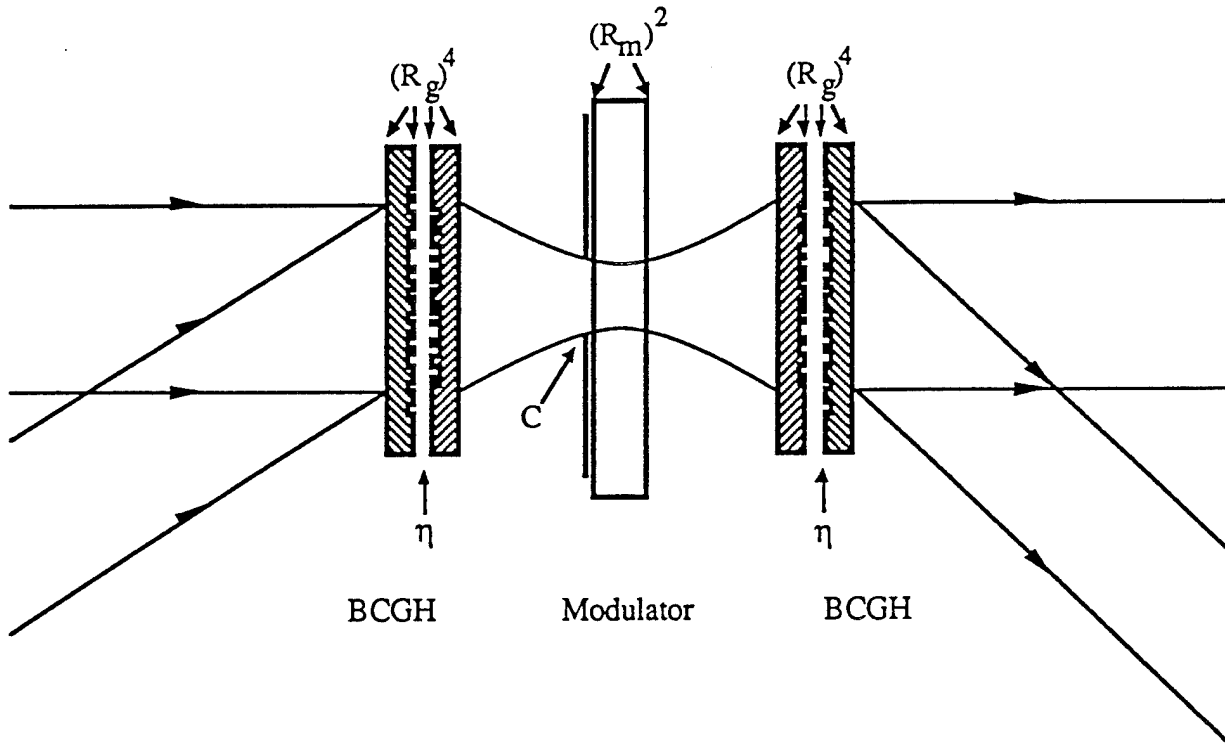


Figure 10: BCGH MIN switching element for circuit switched MIN

Assuming that each optical surface is antireflection coated with a single dielectric layer (to allow maximum range of input angles), and that a 16-level phase hologram is used, then these constants can be estimated to be $\eta = 98.4\%$, $R_g = R_m = 99\%$, and $C = 98.6\%$. The total switch efficiency is then 86.3% , producing an insertion loss of $10\log_{10}[\eta_{\text{switch}}] = -0.638$ db.

(ii) Signal to noise ratio calculation

If the polarization rotation was perfect and the BCGHs distinguished completely between the two polarizations the crosstalk would be zero and the network's SNR would be infinite. Of course, they are not. If the crosstalk coming from one switch is defined to be δ_c , and defining S to be the maximum number of switches in one path and P_o to be the maximum signal strength (when crosstalk is worst), then the SNR of the entire network is given by

$$\begin{aligned} \text{SNR}_{\text{network}} &= \log_{10} \left[\frac{P_o}{P_o \delta_c S} \right] \\ &= \log_{10} \left[\frac{1}{\delta_c} \right] - \log_{10} S \\ &= \beta_c - \log_{10} S \end{aligned}$$

$$\text{Case A} \quad \delta_c = 0.1\% \quad \Rightarrow \quad \beta_c = 30\text{db}$$

$$\text{Case B} \quad \delta_c = 1\% \quad \Rightarrow \quad \beta_c = 20\text{db}$$

These two cases may be typical of BCGH technology for bulk and pixellated BCGH switching elements. We will see in the following section that δ_c is a critical factor that will determine the choice of architecture and maximum network size.

5(b) Architecture comparison results

Table 1 shows the attenuation, SNR, number of stages, and the total number of switches for each of the architectures considered. The last column is the maximum size of the network we may expect to build using BCGH switches with the above technological performance assumptions. The maximum acceptable attenuation was assumed to be 30 db (99.9%) and the minimum SNR was assumed to be 11 db, corresponding to a bit error rate (BER) of 10^{-9} (Ref [10]). Figures 11-13 show the attenuation and SNR for $\beta_c = 30$ and 20 db. Figure 14 shows the total number of switches required for each architecture.

6. Discussion and conclusions

The results indicate that certain types of highly connected networks such as crossbars and MINs are not well suited to implementation with BCGH. However, other networks are very well suited to this implementation. The Batcher Banyon MIN scales up to 256x256 (Figure 6). Both the Benes and Dilated Benes scale beyond 16Kx16K, making them good choices in terms of attenuation limits.

In terms of SNR (Figure 7), when $\beta_s = 30$ db (Case A) the Benes network scales beyond 16K. When β_s is lowered to 20 db (Case B), the crosstalk from the switches along the routing paths severely limit the scalability of these networks (Figure 8) and a dilated network must be used to counter the effect.

Finally in terms of switch count (Figure 9) the Benes MIN has the smallest number of switches ($N[2N\log_2 N - 1]/2$). The dilated Benes has roughly twice this number, while both the crossbar and N-stage require $\mathcal{O}(N^2)$ switches.

In conclusion, we see that the Benes network, which is a rearrangeably non-blocking MIN, is well suited to large-scale implementations of circuit-switched photonic interconnection networks using BCGH switching elements. The network designed uses packet headers to establish the circuit paths

during a dedicated header time interval. The system can use either a centralized controller to determine the appropriate circuit paths or leave the task to the individual input processors to implement a distributed control algorithm. The choice will drive the required smart SLM technology and required pixel complexity or grain size. Finally, the use of a dilated Benes network can alleviate any crosstalk problems that may be characteristic to the pixellated BCGH switch.

- 1 S. Kramer, J. O'Neill, and A. Huang, "Self routing switching network," in Principles of CMOS VLSI Design, N Weste and K. Eshragian, Chapter 9.
- 2 F. Kiamilev, P. Marchand, A. Krishnamoorthy, S. Esener, and S. H. Lee, "Performance comparison between optoelectronic and VLSI multistage interconnection networks," IEEE / OSA Journal of Lightwave Technology, 9(12), December 1991.
- 3 J. Ford and S. Fainman, "Multistage optical interconnects for parallel access shared memories," UCSD Proposal 91-6514 submitted to Rome Air Laboratories.
- 4 G. Broomwell and J. Heath, "Classification categories and historical development of circuit switching topologies," Computing Surveys 15(2), June 1983.
- 5 A. Krishnamoorthy, P. Marchand, F. Kiamilev, and S. Esener, "Grain-size considerations for optoelectronic multistage interconnection networks," Applied Optics .
- 6 T. Cloonan, F. McCormick, and A. Lentine, "Control injection schemes for photonic switching architectures," OSA Technical Digest, Topical Meeting on Photonic Switching, Salt Lake City, March 1991.
- 7 R. Spanke and V. Benes, "N-stage planar optical permutation network," Applied Optics 27(7), pp. 1226-1229, April 1987.
- 8 V. E. Benes, "Growth, complexity and performance of telephone connecting networks," Bell System Technical Journal 62, p. 499, 1983.
- 9 K. Padmanaphan and AZ. Netraveli, "Dilated networks for photonic switching," IEEE Transactions on Communications C-30(12), December 1987.
- 10 Ailawadi, "Photonic switching architectures and their comparison," in Frontiers in Computing Systems Research, Vol. 1, S. Tewksbury Ed., Plenum Press 1990.

Architecture (circuit switched) N inputs / N outputs	Attenuation (worst case optical path loss) α_s = attenuation loss / switch (db)	SNR (worst case signal to noise ratio) β_s = crosstalk isolation/switch (db)	Number of Stages	Number of Switches (in entire network)	Maximum Size
Crossbar (non-blocking)	$(2N-1)\alpha_s$	$\beta_s - 10\log_{10}(N-1)$	N	N^2	16 x 16 (Attenuation limited)
N-Stage Planar (non-blocking)	$N\alpha_s$	$\beta_s - 10\log_{10}N$	N	$\frac{N(N-1)}{2}$	32 x 32 (Attenuation limited)
Batcher-Banyon (non-blocking)	$[1/2\log_2N(\log_2N+1) + \log_2N]\alpha_s$	$\beta_s - 10\log_{10}(\# \text{ of stages})$	$1/2\log_2N(\log_2N+1) + \log_2N$	$\frac{N}{2}[\# \text{ of stages}]$	256 x 256 (Attenuation limited)
Benes (rearrangibly n.-b.)	$(2\log_2N - 1)\alpha_s$	$\beta_s - 10\log_{10}(2\log_2N - 1)$	$2\log_2N - 1$	$\frac{N}{2}[2\log_2N - 1]$	16K x 16K (Att. & SNR limited)
Dilated Benes (rearrangibly n.-b.)	$2(\log_2N)\alpha_s$	∞ (no crosstalk)	$2\log_2N$	$2N\log_2N$	16Kx 16K (SNR limited)

Table 1: Architecture comparison. The network sizes were calculated assuming injection efficiency of -0.638 db (86.3%) and crosstalk of 30 db (0.1%).

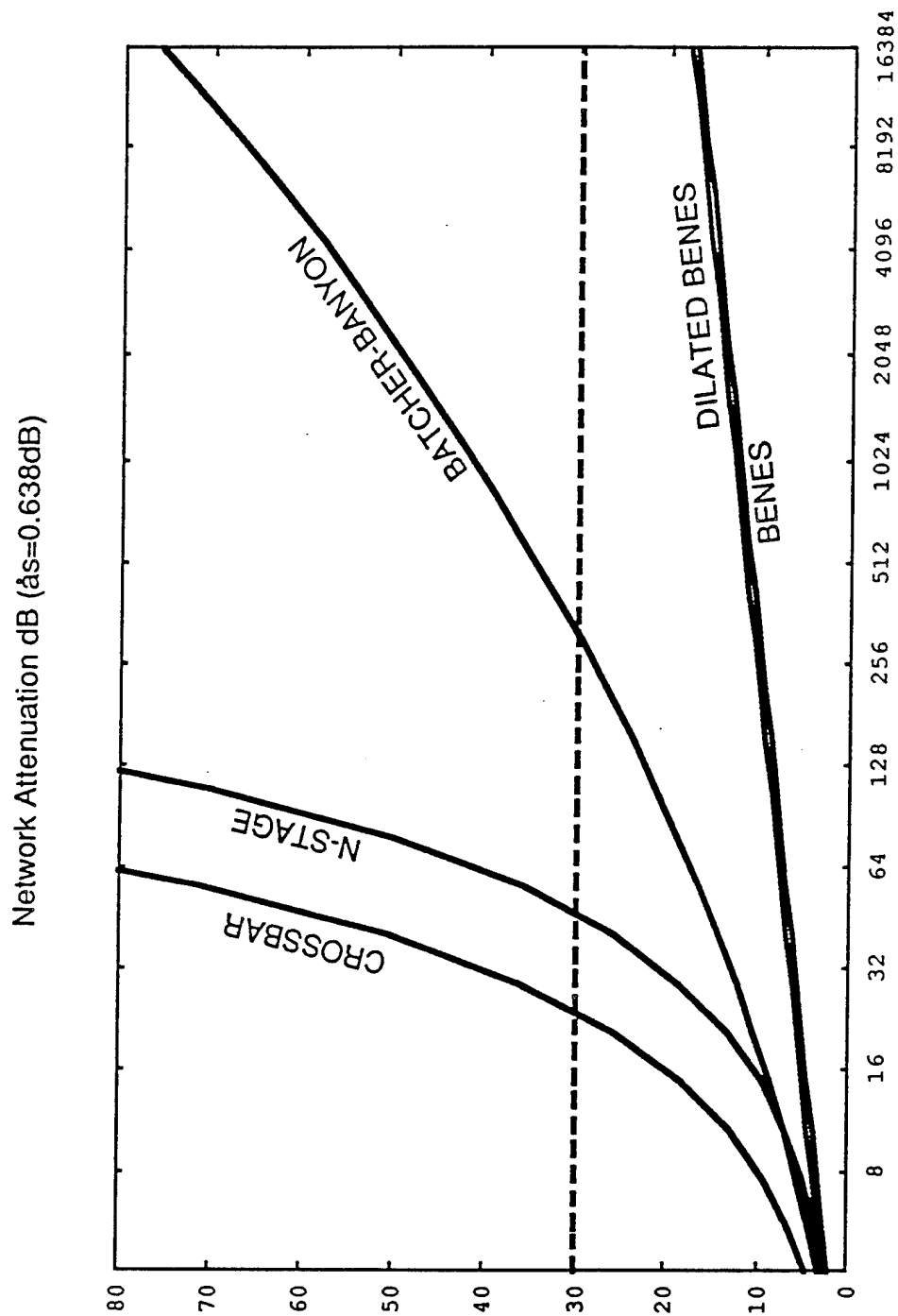


Figure 11: Network attenuation in db, calculated from the formulas in Table 1 using a switch insertion loss of -0.638 db.

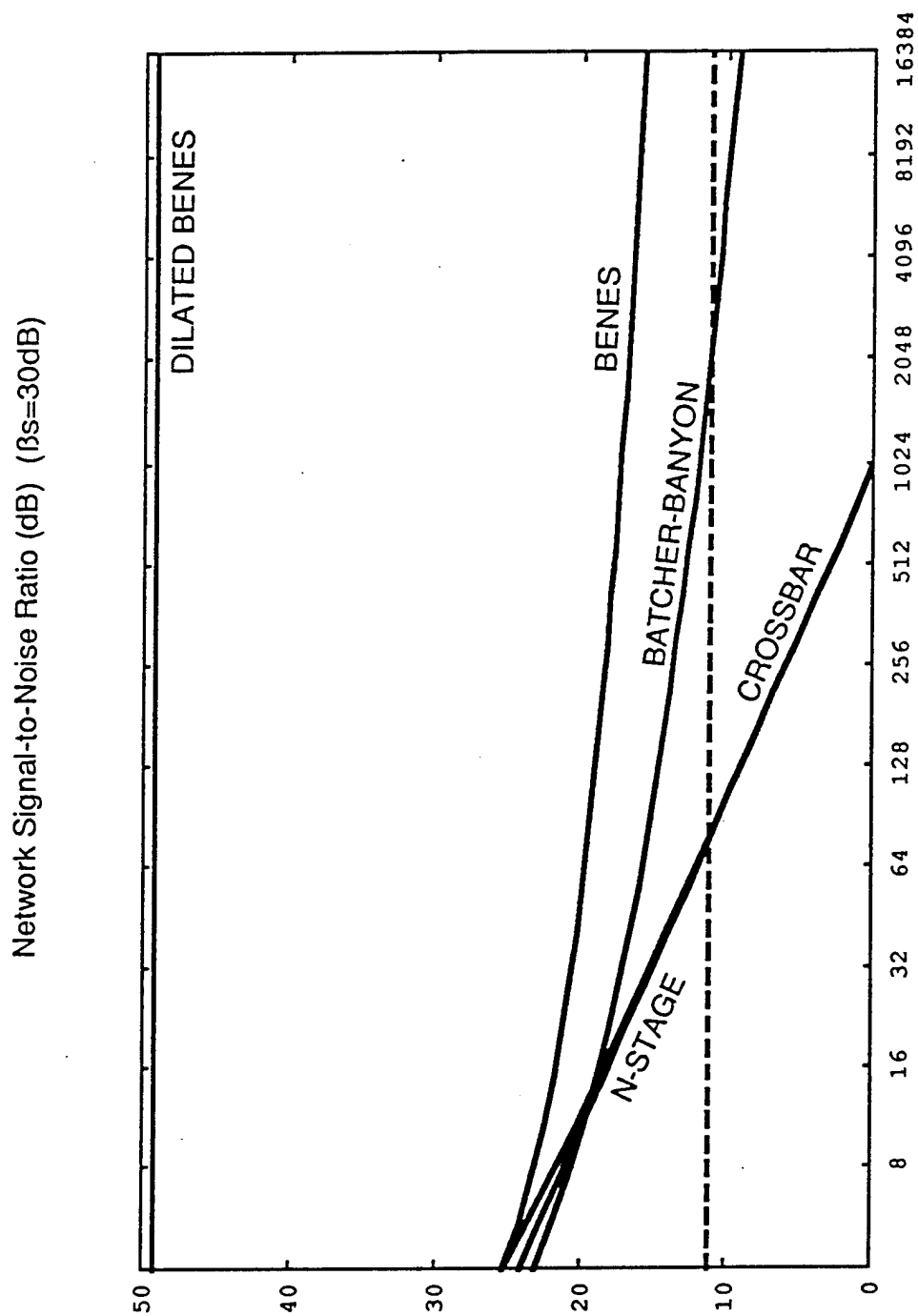


Figure 12: Network signal to noise ratio in db, calculated from the formulas in Table 1 using a switch contrast ratio of 30 db.

Network Signal-to-Noise Ratio (dB) ($\beta_s=20\text{dB}$)

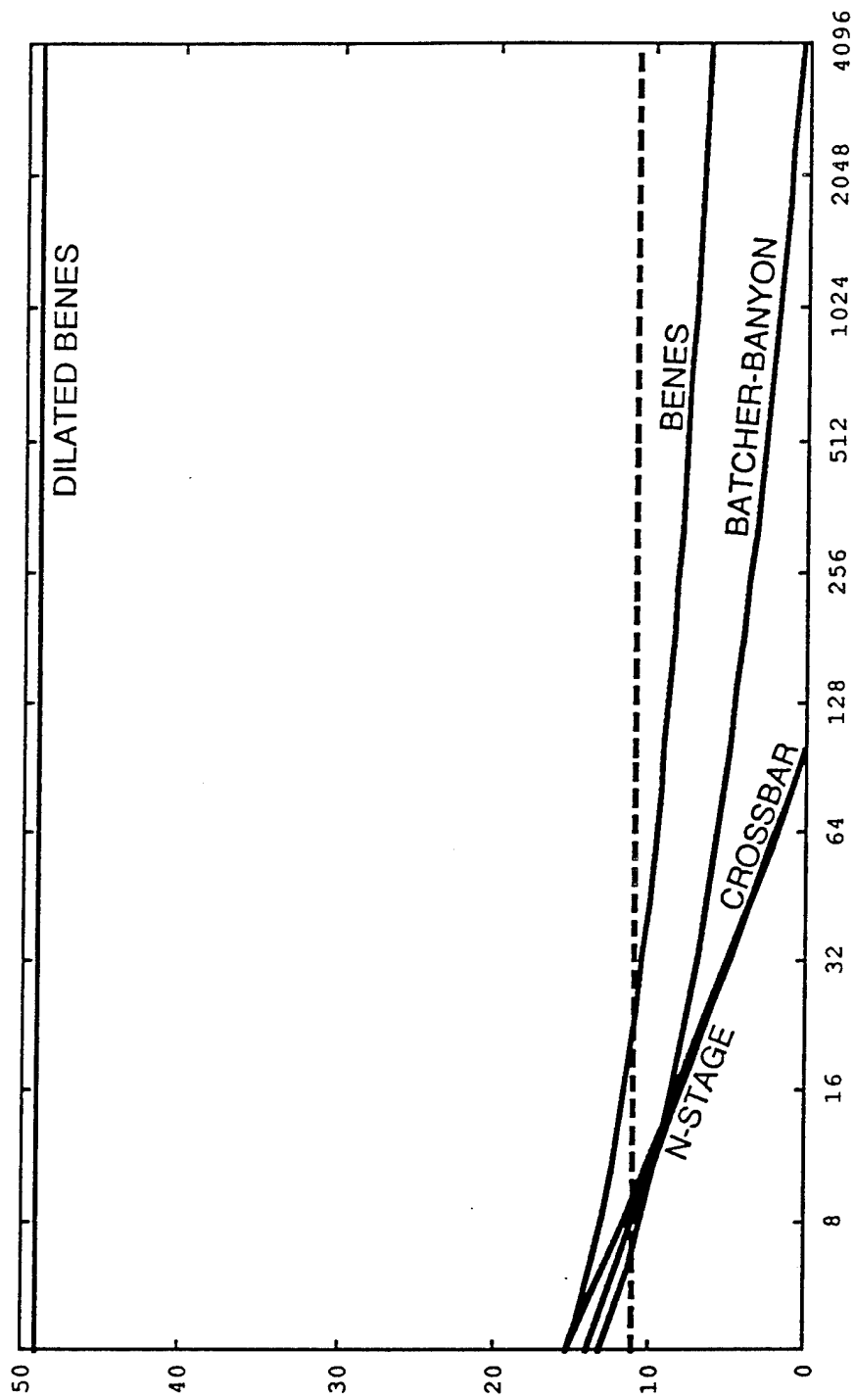


Figure 13: Network signal to noise ratio in db, calculated from the formulas in Table 1 using a switch contrast ratio of 20 db.

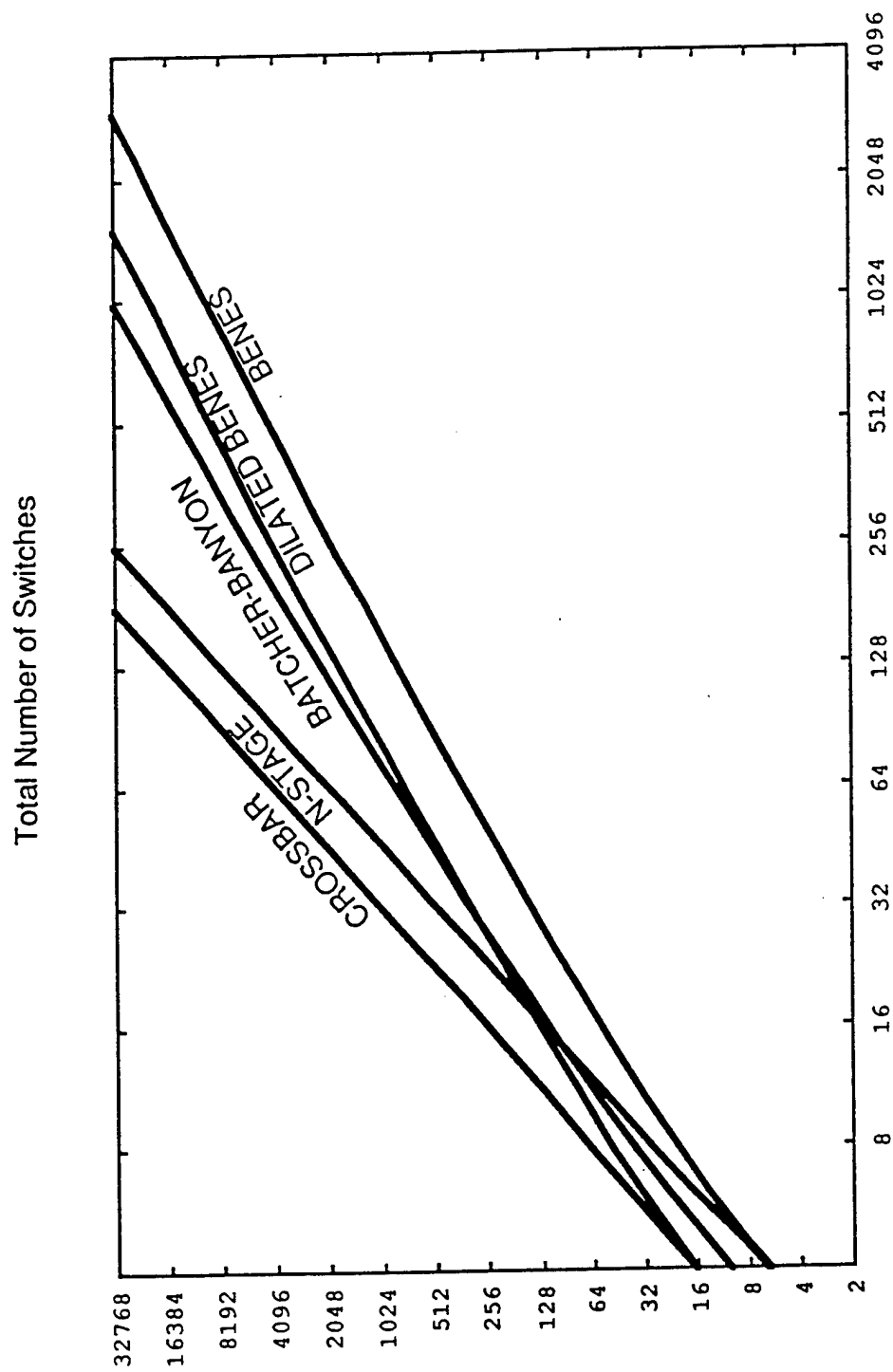


Figure 14: Total number of switches used in the network, calculated from the formulas in Table 1.